

**A USCLIVAR Project to Assess and Compare the Responses of Global Climate Models to  
Drought-Related SST Forcing Patterns: Overview and Results**

Siegfried Schubert<sup>1</sup>, David Gutzler<sup>2</sup>, Hailan Wang<sup>1,3</sup>, Aiguo Dai<sup>4</sup>, Tom Delworth<sup>5</sup>, Clara Deser<sup>6</sup>,  
Kirsten Findell<sup>5</sup>, Rong Fu<sup>7</sup>, Wayne Higgins<sup>8</sup>, Martin Hoerling<sup>9</sup>, Ben Kirtman<sup>10</sup>, Randal Koster<sup>1</sup>,  
Arun Kumar<sup>8</sup>, David Legler<sup>11</sup>, Dennis Lettenmaier<sup>12</sup>, Bradfield Lyon<sup>13</sup>, Victor Magana<sup>14</sup>,  
Kingtse Mo<sup>8</sup>, Sumant Nigam<sup>15</sup>, Philip Pegion<sup>8</sup>, Adam Phillips<sup>6</sup>, Roger Pulwarty<sup>16</sup>, David Rind<sup>17</sup>,  
Alfredo Ruiz-Barradas<sup>15</sup>, Jae Schemm<sup>8</sup>, Richard Seager<sup>18</sup>, Ronald Stewart<sup>19</sup>, Max Suarez<sup>1</sup>, Jozef  
Syktus<sup>20</sup>, Mingfang Ting<sup>18</sup>, Chunzai Wang<sup>21</sup>, Scott Weaver<sup>1,3</sup>, Ning Zeng<sup>15</sup>

- 1 Global Modeling and Assimilation Office, Science and Exploration Directorate, NASA GSFC, Greenbelt, Maryland*  
*2 Department of Earth and Planetary Sciences, University of New Mexico, Albuquerque, New Mexico*  
*3 Goddard Earth Sciences and Technology Center, University of Maryland at Baltimore County, Baltimore, Maryland*  
*4 National Center for Atmospheric Research, Boulder, Colorado*  
*5 National Oceanic and Atmospheric Administration/Geophysical Fluid Dynamics Laboratory, Princeton University, Princeton, New Jersey*  
*6 National Center for Atmospheric Research, Boulder, Colorado*  
*7 Jackson School of Geosciences, The University of Texas at Austin, Austin, Texas*  
*8 Climate Prediction Center, NOAA/NWS/NCEP, Washington, D.C.*  
*9 NOAA Earth System Research Laboratory, Boulder, Colorado*  
*10 Rosenstiel School of Marine and Atmospheric Science, University of Miami, Miami, Florida*  
*11 U.S. Climate Variability and Predictability Research Program, Washington, DC*  
*12 Department of Civil and Environmental Engineering, University of Washington, Seattle, Washington.*  
*13 International Research Institute for Climate and Society, Lamont-Doherty Earth Observatory, Columbia University, Palisades, New York*  
*14 Center for Atmospheric Sciences, National Autonomous University of Mexico, Mexico City, Mexico*  
*15 Department of Atmospheric and Oceanic Science, University of Maryland, College Park, Maryland*  
*16 National Integrated Drought Information System, NOAA, Boulder, CO*  
*17 NASA Goddard Institute for Space Studies, New York, New York*  
*18 Lamont-Doherty Earth Observatory, Columbia University, Palisades, New York*  
*19 Dept of Environment and Geography, University of Manitoba, Winnipeg, Manitoba*  
*20 CSIRO Division of Atmospheric Research, Victoria, Australia*  
*21 Physical Oceanography Division, NOAA/Atlantic Oceanographic and Meteorological Laboratory, Miami, Florida*

12 January 2009

**Submitted to the Journal of Climate for consideration in the USCLIVAR  
Drought Working Group Special Issue**

## Abstract

The USCLIVAR working group on drought recently initiated a series of global climate model simulations forced with idealized SST anomaly patterns, designed to address a number of uncertainties regarding the impact of SST forcing and the role of land-atmosphere feedbacks on regional drought. Specific questions that the runs are designed to address include: What are the mechanisms that maintain drought across the seasonal cycle and from one year to the next? What is the role of the leading patterns of SST variability, and what are the physical mechanisms linking the remote SST forcing to regional drought, including the role of land-atmosphere coupling? The runs were carried out with five different atmospheric general circulation models (AGCMs), and one coupled atmosphere-ocean model in which the model was continuously nudged to the imposed SST forcing. This paper provides an overview of the experiments and some initial results focusing on the responses to the leading patterns of annual mean SST variability consisting of a *Pacific* El Niño/Southern Oscillation (ENSO)-like pattern, a pattern that resembles the *Atlantic* Multi-decadal Oscillation (AMO), and a global *trend* pattern.

One of the key findings is that all the AGCMs produce broadly similar (though different in detail) precipitation responses to the *Pacific* forcing pattern, with a cold *Pacific* leading to reduced precipitation and a warm *Pacific* leading to enhanced precipitation over most of the United States. While the response to the *Atlantic* pattern is less robust, there is general agreement among the models that the largest precipitation response over the U.S. tends to occur when the two oceans have anomalies of opposite sign. That is, a cold *Pacific* and warm *Atlantic* tend to produce the largest precipitation reductions, whereas a warm *Pacific* and cold *Atlantic*

tend to produce the greatest precipitation enhancements. Further analysis of the response over the U.S. to the *Pacific* forcing highlights a number of noteworthy and to some extent unexpected results. These include a seasonal dependence of the precipitation response that is characterized by signal-to-noise ratios that peak in spring, and surface temperature signal-to-noise ratios that are both lower and show less agreement among the models than those found for the precipitation response. Another interesting result concerns what appears to be a substantially different character in the surface temperature response over the U.S. to the *Pacific* forcing by the only model examined here that was developed for use in numerical weather prediction. The response to the positive SST *trend* forcing pattern is an overall surface warming over the world's land areas with substantial regional variations that are in part reproduced in runs forced with a globally uniform SST trend forcing. The precipitation response to the *trend* forcing is weak in all the models.

It is hoped that these early results, as well as those reported in the other contributions to this special issue on drought will serve to stimulate further analysis of these simulations, as well as suggest new research on the physical mechanisms contributing to hydroclimatic variability and change throughout the world.

## 1. Introduction

In recognition of the profound societal impact of drought in many regions of the world and the emerging capabilities in simulating drought with global climate models, the USCLIVAR program initiated a drought working group in 2006 to “*facilitate progress on the understanding and prediction of long-term (multi-year) drought over North America and other drought-prone regions of the world, including an assessment of the impact of global change on drought processes*” (Gutzler and Schubert 2007)”. The specific tasks of the working group were to 1) propose a working definition of drought and related model predictands of drought, 2) coordinate evaluations of existing relevant model simulations, 3) suggest new experiments (coupled and uncoupled) designed to address outstanding uncertainties in the nature of drought, 4) coordinate and encourage the analysis of observational data sets to reveal antecedent linkages of multi-year droughts and 5) organize a community workshop to present and discuss the results.

This paper provides an overview and some results of task (3) of the working group involving the design, coordination, implementation, and initial evaluation of a new set of model simulations that address the roles of sea surface temperature forcing and land-atmosphere feedbacks in the development and maintenance of drought. This work extends and builds upon recent modeling studies (e.g., Hoerling and Kumar 2003, Schubert et al. 2004a and b, Seager et al. 2005, Wang et al. 2008; Wang et al. 2009) as well as numerous observationally-based studies (e.g., Trenberth and Guillemot 1996; Mo et al. 1997, Ting and Wang 1997; Nigam et al. 1999; Koster et al. 2003; Ruiz-Barradas and Nigam, 2004; McCabe et al. 2004; Wang et al. 2006) that have provided substantial insights into the nature of drought and the important role of both the oceans and land-atmosphere

interactions. In particular, this work addresses remaining uncertainties regarding the nature of the physical mechanisms linking remote SST forcing to regional drought, the relative contributions of the different ocean basins and different time scales of SST variability, and the strength of land-atmosphere feedbacks, and thereby starts to frame fundamental questions about the predictability of long-term drought. Specific questions addressed by the working group include: What are mechanisms that maintain drought across the seasonal cycle and from one year to the next? What is the role of the different ocean basins, including the impact of El Niño/Southern Oscillation (ENSO), the Pacific Decadal Oscillation (PDO), the Atlantic Multi-decadal Oscillation (AMO), and warming trends in the global oceans? What is the role of the land? To what extent can droughts develop independently of oceanic variability due to year-to-year memory that may be inherent to the land?

In order to address these questions, the working group proposed that a number of mechanistic experiments be performed that are designed to address some of the key issues outlined above using several different global climate models. A key objective was to be able to assess unambiguously the model dependence of the results. In order to accomplish that, it was proposed that each model be forced with the same set of idealized SST forcing anomalies. In addition, it was proposed that a control run be produced in which each model was forced with the same climatological SSTs. In order to allow an assessment of land-atmosphere feedbacks, an additional set of runs was proposed in which the soil moisture was fixed using a common approach that could be easily implemented in each of the models. The main SST forcing patterns, the experiments, and the models are described in Section 2. Section 3 presents some basic comparisons of the model responses to the leading patterns of SST variability, with a focus on the United States. The summary and conclusions are

given in Section 4. Information on auxiliary experiments and data availability are given in the Appendix.

## **2. The SST Forcing Patterns, Experiments, and Models**

### a) SST forcing patterns

The basic SST data used in this study are the 1901-2004 monthly SST data produced by Rayner et al. 2002). The leading patterns of SST variability are isolated using rotated empirical orthogonal functions (REOFs), where VARIMAX rotation (e.g., Richman 1986) is used to help separate the leading patterns of Pacific and Atlantic SST variability.

The REOFs are computed from global gridded values of annual mean SST for the period 1901-2004. The use of annual means is meant to address the basic question of the nature of the forcing of regional hydroclimates on *interannual* time scales. This of course, does not distinguish between, for example, ENSO and Pacific decadal variability (e.g., Barlow et al. 2001) – the responses to leading SST anomaly patterns that occur on these different time scales is addressed with other supplementary REOFs described in the Appendix.

Figure 1 shows the three leading REOFs and associated principal components (PCs) of the annual mean SST. The first is a global trend pattern, with warming occurring over most of the global ocean. In fact, this spatial pattern can essentially be reproduced by plotting the slopes of the linear trends fit to the 1901-2004 annual mean SST at each grid point (not shown). The associated PC

shows a somewhat more complicated (non-linear) long-term time evolution, showing an almost step-like increase at about 1940, and a clear trend occurring only after the middle 1960s<sup>1</sup>. The second REOF is a pan-Pacific ENSO-like pattern that includes a weak Indian Ocean component. The associated PC shows that this pattern varies on both interannual (ENSO) and decadal time scales, with the latter including the well known shift that occurred in the middle 1970s (e.g., Trenberth and Hurrell 1994). The third REOF is confined for the most part to the North Atlantic Ocean and resembles the Atlantic Multi-Decadal Oscillation pattern (Enfield et al. 2001). The associated PC shows that while this pattern has clear decadal variability it also exhibits considerable interannual variations. These three leading rotated EOFs will in the following be referred to as the *Trend*, *Pacific* and *Atlantic* forcing patterns.

## b) Proposed Experiments

The proposed experiments consist of 50-year<sup>2</sup> simulations in which the model is forced with one or more of the idealized SST anomaly patterns (the *Trend*, *Pacific* and *Atlantic* forcing patterns described above<sup>3</sup>). The full forcing patterns are produced by adding scaled versions of the REOFs to the long-term monthly-varying SST climatology (defined for the period 1901-2004). The scaling factor for the Pacific and Atlantic consists of either plus or minus 2 standard deviations of the associated PCs. This rather large amplitude was chosen to help isolate what in some cases may be rather subtle SST-drought linkages from relatively short model integrations. In the case of the *Trend*, the pattern is scaled by plus or minus 1 standard deviation, which effectively forces the

---

<sup>1</sup> We note that there is considerable sensitivity of the trend pattern to the time period of interest and the datasets used particularly regarding the contribution from the Pacific (e.g., Vecchi et al. 2008; Chen et al. 2008)

<sup>2</sup> The NOAA Global Forecast System Model (GFS) experiments were somewhat shorter (35 years).

model with the 40-year averages of the trend anomalies at the beginning (- 1 standard deviation) and end (+ 1 standard deviation) of the 1901-2004 time period. An additional experiment was proposed to force the models with a globally-uniform SST warming distribution equal to the global mean of the positive trend pattern (0.16°C).

It is important to note that the anomaly patterns are fixed in time and therefore do not have an annual cycle. The absence of a seasonal cycle in the forcing arguably diminishes the importance of winter SST anomalies relative to summer SST anomalies, especially for tropical Pacific variability, because observations indicate that winter anomalies tend to be much larger in magnitude compared to summer anomalies. There is however an annual cycle in the full SST forcing fields as a result of the annual cycle in the climatological SST on which the prescribed anomaly patterns are superimposed. The SST forcing is repeated with no interannual variability for each year of each experiment, but the models still generate interannual variability due to unforced "weather noise" associated with the internal dynamics of the models. We will assess the magnitude of the forced response to prescribed SST anomalies relative to the magnitude of the unforced interannual variability.

The nine baseline experiments of the project consist of the runs in which the models are forced with all eight combinations of the *Pacific* and *Atlantic* patterns shown in Fig. 1, as well as the control run forced only with the monthly varying climatological SST. These are summarized in Table 1 according to the different combinations of patterns and phases of the forcing. For example, PwAc indicates that a model is forced with the warm phase of the *Pacific* and the cold phase of the

---

<sup>3</sup> Masks were applied to REOFs two and three to zero-out any small values that, for the *Pacific* pattern, fall outside the Pacific and Indian Oceans, and that, for the *Atlantic* pattern, fall outside the Atlantic Ocean.

*Atlantic* patterns. In addition to those shown in Table 1, runs were proposed in which the models are forced with either the positive or negative *Trend* pattern, both alone, or superimposed on selected combinations of the *Pacific* and *Atlantic* patterns.

A number of other auxiliary experiments were proposed to isolate further various mechanisms and time scales of variability. Some isolate the role of the tropics, while others attempt to separate the contributions from ENSO and lower frequency Pacific variability. Another set of experiments were formulated to assess the impact of land-atmosphere feedbacks. These additional experiments are described in the Appendix. Another related and important set of experiments consist of AMIP-style simulations (Gates et al. 1999). These are simulations (typically several decades long) in which the models are forced by the historical record of observed SSTs. While the focus of the runs described here is on understanding mechanisms and model sensitivity to idealized SST forcing, the AMIP runs are important in that they facilitate model validation by allowing more direct comparisons of the results with observations.

### c) Contributing groups and models

A number of groups have participated in this project by contributing model runs. While only a few groups have carried out all of the proposed runs, most have done at least the baseline set of experiments defined in Table 1. NASA's Global Modeling and Assimilation Office (GMAO) contributed runs made with version one of the NASA Seasonal-to-Interannual Prediction Project (NSIPP-1) AGCM. NOAA's Climate Prediction Center, with support from the Climate Test Bed, contributed runs made with the Global Forecast System (GFS) AGCM, and NOAA's

Geophysical Fluid Dynamics Laboratory (GFDL) contributed runs made with the AM2.1 AGCM. The Lamont-Doherty Earth Observatory of Columbia University contributed runs made with the NCAR CCM3.0 AGCM, and NCAR contributed runs made with the CAM3.5 AGCM. An additional set of runs was made by COLA/University of Miami with the coupled (atmosphere-ocean) CCSM3.0 model employing a novel adjustment technique to nudge the coupled model towards the imposed SST forcing patterns. The main characteristics of the models of interest and some of the relevant references are presented in Table 2.

### **3. Results**

This section provides an overview of the results from the five AGCMs. Results from the coupled model (CCSM3.0) will be reported on in a separate paper. The main focus here is on the annual mean response over the United States to the *Pacific* SST anomaly pattern. Additional diagnostics are presented that summarize the results from all 8 combinations of the *Pacific* and *Atlantic* forcings shown in Table 1, as well as provide some assessment of the seasonality of the responses. The section ends with a brief overview of the responses to the *trend* pattern.

We begin by examining the ability of the AGCMs to reproduce the observed annual mean precipitation and height field climatologies based on the available AMIP-style simulations (runs forced with observed SSTs) from each model for the period 1980-1998. We note that the results from the AMIP runs are quite similar to those from the control runs (*PnAn* - see Table 1, not shown). The AMIP runs, however, provide a cleaner more direct comparison with observations than the control run, and therefore provide a more useful baseline assessment of model performance.

All the models produce quite reasonable annual mean stationary wave and precipitation patterns (Figure 2). There are, however, differences in the details including such features as the strength of the Pacific ITCZ (c.f. the NSIPP1 and GFS results), and of particular interest here, the strength and orientation of the height anomalies over the Pacific/North American region. In general, the models tend to overestimate precipitation in the western Pacific and Atlantic warm pool regions compared with observations. Most models also tend to underestimate the strength and eastward extent of the east Asian trough. The GFS model is the exception showing a deeper trough together with a stronger ridge over North America compared with the observations and the other models. An interesting feature is the wave train that appears to emanate from the central tropical Pacific and extends across North America into the Atlantic. It appears to be responsible for modifying the structure and amplitude of the west coast ridge and the trough over eastern North America. This feature is evident in the observations and all the models except GFS, where it is at most very weak. The extent to which such differences in the climatological stationary wave pattern impact the response to the SST anomalies is unclear. This issue will be revisited later in the discussions of the model responses.

Figure 3 provides an overview of the agreement between the models with respect to the annual mean responses to the eight combinations of the *Pacific* and *Atlantic* SST patterns. The results are presented as spatial correlations between the 10 different combinations of the 5 models (model 1 correlated with model 2, model 1 correlated with model 3, etc.). The scatter of the 10 different combinations gives a sense of the full range of agreement or disagreement between the various models for any one forcing pattern. The ordinate is the correlation based on

precipitation, and the abscissa is the correlation based on the 200mb height. Figure 3a shows the results for the global and annual mean distributions. Here we limit the comparisons to the 4 basic individual Pacific and Atlantic forcing patterns (no combinations of forcing patterns) to better highlight the differences in the level of agreement between responses to the Pacific and Atlantic forcing patterns. The global annual mean results show a number of interesting features. First, it is clear that the models are in much stronger agreement regarding the responses to the *Pacific* forcing (dark colors), compared with the response to the *Atlantic* forcing (light colors). It is also clear that in general there is more agreement in the height response than in the precipitation response (almost all points lie below the 45° line). For plots 3b-f the results are shown for all 8 forcing patterns. The tropical results (Fig 3b) show generally very strong agreement in the height response for all forcing combinations. The response to the Atlantic forcing shows relatively weak precipitation correlations (generally less than 0.6), while the response to the combined (Pacific and Atlantic) forcing patterns exhibit correlations that are comparable to the Pacific forcing results – a reflection of the dominance of the Pacific forcing. There are also some interesting seasonal differences in the global correlations. The results for DJF (Fig. 3c) show a tendency for greater agreement in the precipitation response than the height response for the cold *Pacific*, while the opposite is true for the warm *Pacific* cases. This seems to reflect a weaker and less robust height response to a cold *Pacific* compared with a warm *Pacific* forcing. The height response appears to be most robust during MAM (Fig. 3d), while JJA shows overall the smallest precipitation correlations. The response to the Atlantic appears to be the most robust (and comparable to the response to the Pacific) during SON (3f).

Figure 4 provides a more in-depth comparison of the annual mean global 200mb height and precipitation responses to the warm *Pacific* (PwAn). The results show considerable large-scale similarity among the models (as expected from the correlations in Figure 3). In particular, all models show the well-known (ENSO-type) horseshoe-shaped precipitation response with a positive precipitation anomaly in the central tropical Pacific surrounded by negative anomalies on either side of the equator. All the models also show negative anomalies over central America, northeastern South America, and the tropical Atlantic. There is general agreement in the height anomalies with wave trains emanating from the tropical Pacific and extending poleward into both hemispheres. The precipitation anomalies over North America appear strongly coupled to the detailed structure of the height anomalies. In particular, the spatial extent of the positive precipitation anomalies over the United States is linked to the orientation and strength of the negative height anomalies over the continent. The response over the U.S. will be discussed further in reference to Figure 6.

Figure 5 shows the global distribution of the responses to the cold *Pacific* (PcAn). The precipitation responses are largely of opposite sign compared with the responses to the PwAn pattern. In particular, all models again show the familiar horseshoe-shaped precipitation response with now a negative precipitation anomaly in the central tropical Pacific surrounded by positive anomalies on either side of the equator. All the models also show positive anomalies over Central America, northeastern South America, and the tropical Atlantic. The height anomalies also tend to be of opposite sign, but in the extratropics they tend to be weaker than the response to the warm *Pacific*, reflecting an asymmetric response to the warm and cold Pacific forcings. All the model responses show a tendency for a split ITCZ (also evident in the PwAn response)

that is most pronounced in the GFDL and CAM3.5 model. All the models also show a ridge over the North Pacific that extends eastward across the United States (though less so for the GFS model).

Figure 6 provides a close-up of the U.S. surface temperature<sup>4</sup> and precipitation responses to the PwAn and PcAn SST patterns. While all the models show a tendency for wet conditions in response to PwAn forcing and dry conditions for the PcAn forcing, there are considerable differences among the models. For example, the NSIPP1 response tends to be relatively localized over the central Great Plains. On the other hand, the largest GFS response occurs along the southern and western tier of states, while the other models tend to show more widespread precipitation anomalies. The surface temperature and precipitation anomalies tend to correspond in the sense that wet anomalies are associated with cold anomalies and dry anomalies are associated with warm anomalies. The temperature response of the GFS model is quite different from the other models, showing extensive warming over much of the US (cooling is confined to the southwest) in response to the PwAn forcing, and only a slight warming over the southern Great Plains in response to the PcAn forcing.

The linkage between the surface temperature and precipitation responses over the central United States is explored further in Figure 7. All the models show a very robust precipitation response with a clear separation of the wet (PwAn) and dry (PcAn) years. There is an overall tendency for a negative relationship between the precipitation and surface temperature anomalies. The exception is again the GFS model, for which the response to the PwAn pattern is generally characterized by positive temperature anomalies and enhanced precipitation. The negative

relationship between the annual mean temperature and precipitation responses is largely a reflection of the warm season responses (primarily JJA but also in some cases MAM and SON, not shown), and presumably reflects a strong tie between the atmosphere and land surface during the warm season for all but the GFS model<sup>5</sup>. Simply put, wetter conditions tend to lead to higher evaporative cooling and thus cooler air temperatures.

Figure 8 summarizes the annual mean responses over the continental U.S. to the 8 different combinations of the *Pacific* and *Atlantic* forcing patterns. Figure 8a shows the precipitation responses. There is agreement among the models that a cold *Pacific* results in a reduction of precipitation, whereas a warm *Pacific* produces precipitation increases. Also, there is general agreement that a warm *Atlantic* leads to reduced precipitation whereas a cold *Atlantic* leads to increased precipitation, though with substantially smaller amplitudes, especially for the response to the cold *Atlantic*. Overall, the models agree that the combination of a cold *Pacific* and warm *Atlantic* (PcAw) tends to produce the largest precipitation deficits, whereas the combination of a warm *Pacific* and cold *Atlantic* (PwAc) tends to produce the largest precipitation surpluses. There is somewhat less agreement for the surface temperature responses (Figure 8b), with generally positive (negative) temperature anomalies associated with precipitation deficits (surpluses), but that is not the case for the GFS model (and to a lesser degree the NSIPP1 model), which shows strong warm anomalies associated with enhanced precipitation (consistent with the previous results).

The scatter in the year-to-year responses to the Pacific forcing shown in Figure 7 for the Great

---

<sup>4</sup> Here and elsewhere in the text the surface temperature over land refers to the skin temperature.

<sup>5</sup> The GFS model is in fact known to have a relatively weak land-atmosphere coupling strength (Koster et al. 2006).

Plains shows the extent to which internal weather variability obscures the signal forced by the SST anomalies. This can be formalized in terms of the quantity

$$R = (\bar{x} - \bar{y})/s_{xy},$$

where  $x$  and  $y$  represent seasonal values from the experiment and control runs respectively, and

the overbar denotes a 50 (35 for the GFS model) year mean. Also,  $s_{xy}^2 = (s_x^2 + s_y^2)/2$ ,

where  $s_x^2$  and  $s_y^2$  are the variance estimates of  $x$  and  $y$ , respectively. The mean difference between the experiment and control (the numerator) is a measure of the signal, so that  $R$  measures the size of the signal in units of standard deviation and can be viewed as the signal to noise ratio associated with the response.

Figure 10 shows  $R$  for the precipitation response to the PwAn and PcAn forcing patterns for each season and all models over different regions of the U.S. (see Figure 9 for the definitions of the regions). The results for the U.S. average (top left panel) show significant (at the 5% level) responses throughout most of the year for both the PwAn and PcAn forcing patterns. Somewhat surprisingly the signal to noise ratio is smallest (in fact only marginally significant) in DJF and largest during MAM/AMJ, when it reaches values of 1.5 or greater. We note that a very similar seasonality is found in the signal itself, so the results do not simply reflect a greater noise during the winter season. We caution however that, as indicated in Section. 2, there is no seasonal cycle in the prescribed forcing, whereas observed SST anomalies are largest in winter.

A comparison of the results for PwAn and PcAn shows that magnitudes are largely comparable with perhaps somewhat weaker  $R$  values (characterized by less agreement among the models)

for the cold Pacific case. The results for the U.S. as a whole reflect, to a large extent, the results in the Great Plains and SW, particularly the southern Great Plains. The northern Great Plains show a similar seasonality, but more modest signal to noise ratios. The NW U.S. has the largest ratios during Northern spring and summer, while there is little evidence for a significant response in the NE. The SE has the largest signal to noise ratios during winter and spring with minimal (not significant) responses during the summer season. In general the models have a very similar seasonality of the response. The GFS model shows a somewhat different behavior especially for the northern Great Plains where the significant response is largely confined to the cold phase during the Fall. Also, in the SE the GFS model differs from the others in that it shows little significant response to the warm phase (PwAn).

Figure 11 shows that the  $R$  values for the surface temperature response are substantially different from those for precipitation. In addition to having generally smaller amplitudes, there is considerable disagreement among the models regarding the seasonality and even the sign of  $R$ . For the continental U.S. as a whole (top left panel) the response to the warm Pacific is significant for 3 models during the warm season (May – August), and large and significant for one model (GFS) during the cold season (March – May). The latter result reflects the unusual (compared to the other models) southward extension of the upper level high in the GFS response (e.g., Figure 4), and can be traced to the large signal-to-noise ratios in the northern tier of states (the second, third and fourth top panels of Figure 11). The response to the cold Pacific is for the most part not significant or marginally significant, with the largest values occurring during late summer and fall. Excluding the GFS model, the most consistent results and largest  $R$  values occur for the southern tier of states (bottom panels of Figure 11). For example, the southern Great Plains

show a consistent warming signal during the warm season in response to a cold *Pacific* (with  $R$  peaking in late spring), and cold anomalies in response to a warm *Pacific* beginning in late winter and extending into late summer. The southwest shows considerable asymmetry in the cold and warm Pacific responses, with only marginally significant responses to a cold *Pacific* whereas the response to the warm *Pacific* shows significant  $R$  values for two of the models during late spring and early summer. In the southeast (bottom right panel of Figure 11) all the models agree on having little skill during the late summer to early winter seasons in response to the cold *Pacific*. Four models show a tendency for a significant warming in late spring and early summer in response to the cold *Pacific*, while three models show cooling during the summer in response to the warm *Pacific*.

Finally, we present a brief overview of the responses of the models to the trend pattern. The focus is on the surface temperature response to the positive trend pattern and the results are compared to those from the companion set of runs in which the models were forced with a globally uniform SST warming of  $0.16^{\circ}\text{C}$ . The precipitation response to the *trend* (not shown) is weak for all the models, with anomalies that exceed  $0.5$  mm/day in amplitude largely confined to a few locations in the tropical Pacific and Indian Oceans. The basic response of all the models (left panels of Figure 12) is a tendency for warming over most of the world's land areas, though there are substantial regional variations that differ between models. The GFS and GFDL models show the strongest warming, with especially large values (exceeding  $0.5^{\circ}\text{C}$ ) concentrated over North America and parts of Asia and Australia. CAM3.5 and CCM3 show the weakest warming, while the NSIPP1 model shows intermediate values with the largest warming occurring over North America. Focusing on North America, the GFS model shows strong warming over most

of the continent (especially the western half), while the GFDL and NSIPP1 models show warming that is more confined to the central and eastern United States. All but the GFS model show a substantial area of cooling spanning much of northern Canada and Alaska.

The impact of any regional variations in the SST *trend* forcing pattern can be deduced from comparisons with the runs forced by the globally uniform warming pattern<sup>6</sup> (right panels of Figure 12). The comparison shows that many of the features of the response to the *trend* pattern are reproduced in the response to uniform warming. For example, some of the enhanced warming over North America in the GFS model, the enhanced warming over Asia in the GFDL model, and more generally, the spatial pattern of the warming over much of Asia in all the models, is reproduced in the uniform warming case. The global spatial correlations between the responses to the *trend* and uniform warming of the annual mean values over land range from 0.34 for the NSIPP model to 0.43 for the GFDL model. There is, however, a large seasonal variation in the correlations for some models. For example, for the GFDL model, the correlations ranging from 0.7 in March to 0.15 in July. A key difference between the two sets of responses over North America is that the cooling in Northern Canada and Alaska noted earlier does not show up in the response to the uniform warming, indicating that this feature is primarily the result of regional variations in the SST *trend* pattern. Also, the localized warming responses over the U.S. in the GFDL and NSIPP models are not reproduced in the case of uniform warming.

#### **4. Summary and Discussion**

The USCLIVAR drought working group recently initiated a coordinated (multi-institutional and multi-model) effort to produce a set of idealized simulations designed to address fundamental questions regarding the physical mechanisms that link SST variations to regional drought, including an assessment of the role of land-atmosphere feedbacks. The set of experiments consist of multiyear simulations in which the models were forced by a number of idealized SST forcing patterns consisting of the leading rotated EOFs of SST variability on interannual and longer time scales. The main set of EOF forcing patterns include a global *trend* pattern, a *Pacific* ENSO-like pattern, and an *Atlantic* pattern that resembles the Atlantic Multi-Decadal Oscillation. Additional SST forcing patterns were designed to isolate ENSO and longer (decadal) time scales, and to isolate the influence of the tropical SST. A number of groups also ran experiments in which the land-atmosphere interactions were disabled by prescribing the soil moisture.

This paper, in addition to providing a general overview of the project, attempts to provide a broad-ranged assessment of the model results focusing on overall behavior and highlighting where the models tend to agree and disagree. Results are limited to the responses to the two leading *Pacific* and *Atlantic* forcing patterns. While showing some aspects of the global-scale response, much of the focus of this paper is on the responses over the continental United States.

A number of key results emerge from this initial analysis of the experiments. First, all the models produce similar (though different in detail) precipitation anomalies over the continental United States in response to the *Pacific* forcing pattern, with a tendency for reduced precipitation when forced with a cold Pacific and a tendency for enhanced precipitation when forced with a

---

<sup>6</sup> This run was not done with CAM3.5.

warm Pacific. The response to the *Atlantic* pattern is not as robust as the response to the *Pacific*, though there is a tendency for reduced precipitation when forced with a warm *Atlantic* and a tendency for enhanced precipitation when forced with a cold *Atlantic*. There is general agreement among the models that the largest precipitation response over the continental United States tends to occur when the two oceans have anomalies of opposite sign. That is, a cold *Pacific* and warm *Atlantic* tend to produce the largest precipitation reductions, whereas a warm *Pacific* and cold *Atlantic* tend to produce the greatest precipitation enhancements.

The models tend to agree less on the area mean U.S. surface temperature response to both the *Atlantic* and *Pacific* forcing, though (with the exception of the GFS model) there is a general tendency for wet conditions to be associated with cold surface temperature anomalies and dry conditions to be associated with warm surface temperature anomalies. This greater disagreement for the surface temperature response appears to be the result of the sensitivity of the response over the U.S. to small (on planetary scales) shifts in the upper level wave response to the SST forcing. This is less so for the precipitation response. It is not clear exactly why that is the case, though it may be partly that the area mean of the more localized precipitation anomalies is less sensitive to shifts in the planetary wave forcing. The model differences are highlighted by the GFS response to the warm *Pacific* SST forcing, which tends to place the upper level ridge of the response over North America considerably further south compared to the other models, leading to warm surface temperature anomalies that extend well into the southern tier of states.

Another key area of agreement among the models is in the seasonality of the signal-to-noise ratio ( $R$ ) of continental U.S. precipitation associated with the *Pacific* forcing. All the models show

that the largest  $R$  values occur in spring with surprisingly small (not significant)  $R$  values during winter. The above results for the U.S. as a whole, reflect those in the Great Plains and the southwest, particularly the southern Great Plains. In contrast to these results, the  $R$  values of the surface temperature response to the *Pacific* forcing are generally lower and show considerably less agreement among the models. For the continental U.S. as a whole the GFS model stands out as having very high  $R$  values during the cold season (March – May). This again appears to reflect the unusual (compared to the other models) southward extension of the upper level high in the GFS response and can be traced to the large  $R$  values that occur in the northern tier of states. For the other models, the most consistent results and largest  $R$  values occur for the southern tier of states, with, for example, the southern Great Plains showing a consistent warm anomaly during the warm season in response to a cold *Pacific* (with  $R$  peaking in late spring), and cold anomalies in response to a warm *Pacific* beginning in late winter and extending into late summer.

The surface temperature response to the positive SST global *trend* forcing pattern shows substantial regional variations that are in part reproduced in runs forced with a globally uniform SST trend forcing. There is however substantial disagreement among the models in the regionality (e.g., the enhanced surface temperature response produced over North America by some of the models), highlighting the challenge of predicting regional impacts of global warming. The precipitation response to the *trend* forcing was found to be weak in all the models.

The differences in the responses to the *Pacific* forcing pattern over the U.S. between the GFS and the other models is intriguing. Understanding these differences is important in view of the critical role that the GFS model (as part of the NOAA Climate Forecast System) plays in seasonal prediction, and more generally the increasingly important role that climate models play in providing information on the regional impacts of global climate variability and change. While it is beyond the scope of this paper to fully address the reasons for these differences, it appears likely that the differences in the stationary wave patterns play a role. The GFS model produces a very reasonable stationary wave pattern and arguably produces the most realistic overall structure of the Pacific trough and North American ridge (Figure 2). The North American ridge is, however, stronger and the trough to the east considerably weaker compared with the other models and the observations. A preliminary linear model analysis of the NSIPP1 model stationary waves (results not shown) indicates that the eastern North American trough is particularly sensitive to the heating in the western tropical Pacific, suggesting that the differences we see in the climatological precipitation in that region may play an important role. On the other hand, most of the other models produce a rather weak Pacific trough - a problem that very likely also contributes to deficiencies in the response over North America. Clearly more work is needed to not only improve our understanding of the sensitivity of stationary waves to the climatological forcing, but also to determine the extent to which that sensitivity translates into uncertainties in the extratropical response to SST anomalies.

The results of this initial analysis of the model experiments serve to highlight and quantify the important role of SST anomalies (especially those in the Pacific) in generating drought and pluvial conditions over the United States. The differences between the model results provide an

assessment of the current uncertainties in our ability to model the global response to SST forcing (including the feedbacks associated with land-atmosphere interactions) and reinforce the need to improve our climate models. We expect that these results, as well as those reported in the other contributions to this special issue on drought will serve to stimulate further analysis of the simulations, as well as suggest new research on the physical mechanisms contributing to hydroclimatic variability and change throughout the world.

*Acknowledgements:* This project was carried out as part of a U.S. CLIVAR drought working group activity supported by NASA, NOAA, and NSF to coordinate and compare climate model simulations forced with a common set of idealized SST patterns. The authors would like to thank NASA's Global Modeling and Assimilation Office (GMAO) for making the NSIPP1 runs available, the Lamont-Doherty Earth Observatory of Columbia University for making their CCM3 runs available, NOAA's Climate Prediction Center (CPC)/Climate Test Bed (CTB) for making the GFS runs available, NOAA's Geophysical Fluid Dynamics Laboratory (GFDL) for making the AM2.1 runs available, the National Center for Atmospheric Research (NCAR) for making the CAM3.5 runs available, and the Center for Ocean Land Atmosphere (COLA) and the University of Miami's Rosenstiel School of Marine and Atmospheric Science for making the CCSM3.0 coupled model runs available. The NASA/GMAO contributions to this project were supported by funding from the NASA Energy and Water cycle Study (NEWS) program, and the NASA Modeling and Analysis Program (MAP).

## Appendix A: Auxiliary Experiments

In addition to forcing the models with the three main SST patterns presented in the text (the *Pacific*, *Atlantic*, and *trend*), the participating groups were encouraged to force their models with other patterns consisting of the tropical-only version of the *Pacific* and *Atlantic* patterns, and low and high frequency versions of the *Pacific* SST patterns. Details about these patterns are discussed below.

In order to differentiate between the impacts of the tropics and extratropics, another set of SST “tropical” forcing patterns was produced based on the interannual *Pacific* and *Atlantic* patterns. For the Pacific case, this was done by linearly tapering the values to zero between 15° and 21° latitude. The taper is such that the full amplitude occurs at 15°, ½ of the full amplitude remains at 18°, and the anomaly is identically zero from 21° latitude to the pole. Also, the meridional edges are such that the western boundary occurs at 120°E. For the Atlantic case, the *Atlantic* pattern was modified so that the edges of the box with the full anomalies were chosen as 88°W to 13°W, and 12°N to 18°N. The anomalies were tapered linearly north and south, with latitudes 9°N and 21°N getting 1/2 the anomaly, and with the anomaly going to 0 at latitudes 6°N and 24°N.

In addition to the patterns described above (based on annual mean SST), two other patterns were produced for the Pacific that attempt to separate the ENSO and longer-term patterns of variability. The long time scales were isolated by applying a filter to the monthly SST data that retains time scales of about 6 years and longer (Zhang et al. 1997). The high (residual) frequencies (shorter than 6 years) were obtained by subtracting the low

frequency filtered data from the unfiltered monthly data. The leading REOFs and associated PCs from both the low pass (time scales of 6 years and longer) and residual (time scales shorter than 6 years) data are shown in Figure A1. In the case of the low-pass we focus on the second REOF (the first is again the trend pattern shown in Figure 1). The second low frequency REOF shows the well-known meridionally extensive pan-Pacific decadal pattern of variability (e.g., Barlow et al. 2001), with substantial middle latitude amplitude that in the Northern Hemisphere is linked to the Pacific Decadal Oscillation (Zhang et al 1997). In contrast, the leading REOF of the residual (high frequency) SST shows a clear ENSO structure with significant amplitudes that are largely confined to the central and eastern equatorial Pacific.

A final set of experiments was designed to assess the impact of soil moisture feedbacks. In this case archives of standard multi-decadal AMIP-style simulations were used to derive the climatological seasonal cycles of soil moisture content for each soil layer at each land point on the globe. Here weekly resolution was preferred, but in cases where these were not available monthly data were used. Subsets of the above idealized SST simulations were then repeated in such a way that at each time step, the simulated soil moisture states were thrown out and replaced with states interpolated from the climatological values established in the first simulation. Details of the various experiments and other information and links relevant to the USCLIVAR drought working group project may be found at:

[http://gmao.gsfc.nasa.gov/research/clivar\\_drought\\_wg/index.html](http://gmao.gsfc.nasa.gov/research/clivar_drought_wg/index.html)

## References

- Adler, R.F., G.J. Huffman, A. Chang, R. Ferraro, P. Xie, J. Janowiak, B. Rudolf, U. Schneider, S. Curtis, D. Bolvin, A. Gruber, J. Susskind, P. Arkin, 2003: The Version 2 Global Precipitation Climatology Project (GPCP) Monthly Precipitation Analysis (1979-Present). *J. Hydrometeor.*, 4,1147-1167.
- Bacmeister, J., P.J. Pegion, S. D. Schubert, and M.J. Suarez, 2000: An atlas of seasonal means simulated by the NSIPP 1 atmospheric GCM, NASA Tech. Memo. No. 104606, volume 17, Goddard Space Flight Center, Greenbelt, MD 20771, 2000.
- Barlow, M., S. Nigam, and E.H. Berbery, 2001: ENSO, Pacific Decadal Variability, and U.S. summertime precipitation, drought, and streamflow. *J. Climate*, 14, 2105-2128.
- Bonan, G.B., 1996: The NCAR land surface model (LSM version 1.0) coupled to the NCAR community climate model. Technical Report NCAR/TN-429 + STR, NCAR Boulder, Colorado.
- Campana, K. and P. Caplan, Editors, 2005: Technical Procedure Bulletin for T382 Global Forecast System  
[http://www.emc.ncep.noaa.gov/gc\\_wmb/Documentation/TPBoct05/T382.TPB.FINAL.htm](http://www.emc.ncep.noaa.gov/gc_wmb/Documentation/TPBoct05/T382.TPB.FINAL.htm).

- Chen J., A. D. Del Genio, B. E. Carlson, and M. G. Bosilovich, 2008: The spatiotemporal structure of twentieth-century climate variations in observations and reanalyses. Part I: Long-term trend. *J. Climate*, 21, 2611–2633.
- Collins, W. D., and co-authors, 2006a: The Community Climate System Model version 3 (CCSM3). *J. Climate*, 19, 2122-2143.
- Delworth et al., 2006. GFDL's CM2 global coupled climate models - Part 1: Formulation and simulation characteristics, *J. Climate*, 19, 643-674.
- Ek, M, K. E. Mitchell, Y. Lin, E. Rogers, P. Grunmann, V. Koren, G. Gayno and J. D. Tarpley, 2003: 'Implementation of Noah land surface model advances in the National Centers for Environmental Prediction operational mesoscale Eta model', *JGR*, Vol. 108, No. D22, 8851, doi:10.1029/2002JD003296 .
- Enfield, D., A. Mestas-Nuñez, and P. Trimble, 2001: The Atlantic Multidecadal Oscillation and its relation to rainfall and river flows in the continental U.S. *Geophys. Res. Lett.*, **28**, 2077-2080.
- Gates, W.L., J.S. Boyle, C. Covey, C.G. Dease, C.M. Doutriaux, R.S. Drach, M. Fiorino, P.J. Gleckler, J.J. Hnilo, S.M. Marlais, T.J. Phillips, G.L. Potter, B.D. Santer, K.R. Sperber, K.E. Taylor, and D.N. Williams, 1999: An overview of the results of the Atmospheric Model Intercomparison Project (AMIP I). *Bulletin of the American Meteorological Society*, **80(1)**, 29-55.

Gutzler, D. and S. Schubert: The U.S. CLIVAR Working Group on Long-Term Drought,”  
U.S. CLIVAR *Variations* (Spring 2007, volume 5, No. 1).

Hack J. J., 1994: Parameterization of moist convection in the National Center for Atmospheric  
Research Community Climate Model (CCM2). *J. Geophys. Res.*, 99, 5551–5568.

Hoerling, M.P. and A. Kumar, 2003: The perfect ocean for drought. *Science*, 299, 691-699.

Kalnay, E., and Coauthors, 1996: The NCEP/NCAR 40-year reanalysis project. *Bull.  
Amer.Meteor.Soc.*, 77, 437-471.

Kiehl, J.T., J.J. Hack, G. Bonan, B.A. Boville, D. Williamson and P. Rasch, 1998. The National  
Center for Atmospheric Research Community Climate Model: CCM3. *J. Climate*,  
\*11\*, 1131-1149.

Koster, R.D. and M.J. Suarez, 1996: Energy and water balance calculations in the Mosaic  
LSM, NASA Tech. Memo. 104606, vol. 9, pp194.

Koster R. D., M. J. Suarez, R. W. Higgins, and H. Van den Dool. 2003: Observational evidence  
that soil moisture variations affect precipitation. *Geophys. Res. Lett.*, 30, 1241,  
doi:10.1029/ 2002GL016571.

Koster, R.D., P. A. Dirmeyer, Z. Guo, G. Bonan, E. Chan, P. Cox, C. T. Gordon, S. Kanae, E.  
Kowalczyk, D. Lawrence, P. Liu, C-H Lu, S. Malyshev, B. McAvaney, K. Mitchell, D.  
Mocko, T. Oki, K. Oleson, A. Pitman, Y. C. Sud, C. M. Taylor, D. Verseghy, R. Vasic,

- Y. Xue, T. Yamada, 2006: GLACE: The Global Land–Atmosphere Coupling Experiment. Part I: Overview, *J. Hydrometeor.*, 7, pages 590–610.
- McCabe, G. J., Palecki, M. A., and Betancourt, J. L. 2004. Pacific and Atlantic Ocean influences on multidecadal drought frequency in the United States. *Proceedings of the National Academy of Sciences* 101, p. 4136-4141.
- Milly, P. C. D., and A. B. Shmakin, 2002. Global modeling of land water and energy balances. Part I: The land dynamics (LaD) model. *J. Hydrometeorology*, 3, 283-299.
- Mo, K.C., J.N. Paegle, and R.W. Higgins, 1997: Atmospheric Processes Associated with Summer Floods and Droughts in the Central United States. *J. Climate*, 10, 3028–3046.
- Moorthi, S. and M. J. Suarez, 1992: Relaxed Arakawa-Schubert: A parameterization of moist convection for general circulation models. *Mon. Wea. Rev.*, 120, 978-1002.
- Nigam, S., M. Barlow, and E.H. Berbery, 1999: Pacific decadal SST variability: Impact on U.S. drought and streamflow. *Eos, Transactions, American Geophysical Union*, Vol. 80, 51 (Dec. 21), 621-625.
- Oleson, K. W., G.-Y. Niu, Z.-L. Yang, D.M. Lawrence, P. E. Thornton, P. J. Lawrence, R. Stockli, R. E. Dickinson, G. B. Bonan, S. Levis, A. Dai and T. Qian, 2008:

Improvements to the Community Land Model and their impact on the hydrological cycle. *J. Geophys. Res.*, 113, G01021, doi:10.1029/2007JG000563.

Rayner, N.A., D.E. Parker, E.B. Horton, C.K. Folland, L.V. Alexander, D.P. Rowell, E.C.

Kent, A. Kaplan, 2002: Global analyses of SST, sea ice and night marine air temperature since the late nineteenth century. *J. Geophys. Res.* **108**, 4407, doi:10.1029/2002JD002670 (2003).

Richman M.B., 1986. Rotation of principal components. *J. Climatol.*, 6, 293–335.

Ruiz-Barradas, A. and S. Nigam, 2004: Warm Season Rainfall Variability over the U.S. Great Plains in Observations, NCEP and ERA-40 Reanalyses, and NCAR and NASA Atmospheric Model Simulations. *J. Climate*, 18, 1808- 1830.

Schubert,S.D., M.J. Suarez, P.J. Pegion, M.A. Kistler, and A. Kumer, 2002: Predictability of zonal means during boreal summer," *J.Climate*, 15, 420-434.

Schubert, S.D. M.J. Suarez, P.J. Pegion, R. D. Koster, and J.T. Bacmeister, 2004a: Causes of long-term drought in the U.S. Great Plains, *J.Climate*, 17, 485-503.

Schubert S. D., M. J. Suarez, P. J. Pegion, R. D. Koster, and J. T. Bacmeister. 2004b: On the Cause of the 1930s Dust Bowl. *Science*, 303, 1855 – 1859, DOI: 10.1126/science.1095048.

Seager, R., Y. Kushnir, C. Herweijer, N. Naik, and J. Velez: 2005, Modeling of tropical forcing of persistent droughts and pluvials over western North America: 1856-2000. *J. Climate*, 18, 4068–4091.

Stockli, R., D. M. Lawrence, G.-Y. Niu, K. W. Oleson, P. E. Thornton, Z.-L. Yang, G. B. Bonan, A. S. Denning, and S. W. Running, 2008: Use of FLUXNET in the Community Land Model development, *J. Geophys. Res.*, 113, G01025, doi:10.1029/2007JG000562.

The GFDL Global Atmospheric Model Development Team, 2004. The New GFDL Global Atmosphere and Land Model AM2-LM2: Evaluation with Prescribed SST Simulations. *J. Climate*, 17, 4641-4673.

Ting, M. and H. Wang, 1997: Summertime U.S. precipitation variability and its relation to Pacific Sea Surface Temperature, *J. Climate*, 10,1853-1873.

Trenberth, K.E. and J.W. Hurrell, 1994: Decadal atmosphere-ocean variations in the Pacific. *Climate Dynamics*, 9, 303-319.

Trenberth, K.E. and C.J. Guillemot, 1996: Physical processes involved in the 1988 drought and 1993 floods in North America. *J. Climate*, 9, 1288-1298.

- Vecchi, A. G., A. Clement, and B. J. Soden, 2008: Examining the tropical Pacific's response to global warming. *EOS, Trans. Amer. Geophys. Union*, **89** (9), pp. 81, 83.
- Wang, C., D. B. Enfield, S.-K. Lee, and C. W. Landsea, 2006: Influences of the Atlantic warm pool on Western Hemisphere summer rainfall and Atlantic hurricanes. *J. Climate*, **19**, 3011-3028.
- Wang, C., S.-K. Lee, and D. B. Enfield, 2008: Climate response to anomalously large and small Atlantic warm pools during the summer. *J. Climate*, **21**, 2437–2450.
- Wang, H., S. Schubert, M. Suarez, J. Chen, M. Hoerling, A. Kumar, P. Pegion, 2009: Attribution of the seasonality and regionality in climate trends over the United States during 1950-2000. Accepted in *J. Climate*.
- Zhang G. J., and N. A. McFarlane, 1995: Sensitivity of climate simulations to the parameterization of cumulus convection in the Canadian Climate Centre general circulation model. *Atmos.–Ocean*, **33**, 407–446.
- Zhang, Y., J. M. Wallace, and D. S. Battisti, 1997: ENSO-like interdecadal variability. *J. Climate*, **10**, 1004 –1020.

## List of Figures

Figure 1: The three leading rotated EOFs (left panels) and associated PCs (right panels) of the annual mean SST based on the period 1901-2004. The values are scaled so that the product of the PCs and EOFs gives units of °C. The Pacific and Atlantic patterns reflect the two standard deviation forcing amplitude applied to the models, while the trend pattern must be divided by a factor of two to obtain the forcing amplitude.

Figure 2: Annual mean precipitation and 200mb eddy height field averaged over the years 1980-1998. The model results are from AMIP-style runs from each model (runs forced by observed SSTs). For the observations (lower right panel), the precipitation is from GPCP (Adler et al. 2003) and the height fields are from the NCEP/NCAR reanalyses (Kalnay et al. 1996). The time period was chosen in order to have a common set of years for each model. Contour interval for the height field is 20m (negative values are dashed and the zero line is the first solid contour). Precipitation is in mm/day

Figure 3: Spatial correlations of precipitation anomalies (ordinate) versus spatial correlations of 200mb height anomalies (abscissa) for the various combinations of models and for the 8 combinations of forcing for the Pacific and Atlantic patterns. a) global correlations of annual means, b) tropical correlations ( $\pm 30^\circ$  latitude) of annual means, c) global correlations for DJF d) global correlations for MAM, e) global correlations for JJA, and f) global correlations for SON. See text for details. The colors refer to the forcing patterns indicated along the bottom of the plots.

Figure 4: Annual mean 200mb height and precipitation responses to the of PwAn SST anomaly pattern. The anomalies for each model are computed with respect to its annual mean response to a simulation in which the model is forced with climatological SSTs. See text for details on the SST forcing. Contour interval for height is 10 meters (negative values are dashed and the zero line is the first solid contour). Unit for precipitation is mm/day.

Figure 5: Annual mean 200mb height and precipitation responses to the of PcAn SST anomaly pattern. The anomalies for each model are computed with respect to its annual mean response to a simulation in which the model is forced with climatological SSTs. See text for details on the SST forcing. Contour interval for height is 10 meters (negative values are dashed and the zero line is the first solid contour). Unit for precipitation is mm/day.

Figure 6: Annual mean surface temperature (top panels, units: °C/day) and precipitation (bottom panels, units: mm/day) responses to the PwAn (left panels) and PcAn (right panels) SST anomaly pattern. The anomalies for each model are computed with respect to its annual mean response to a simulation in which the model is forced with climatological SSTs. See text for details on the SST forcing.

Figure 7: Scatter plots of the Great Plains annual mean precipitation (ordinate) versus surface temperature (abscissa) response to the PwAn (red dots) and PcAn (blue dots) SST anomaly patterns for the Great Plains area average. Each point represents one of 50 (35 for the GFS model) years of each run.

Figure 8: The annual and continental United States mean responses for a) precipitation and b) surface temperature for all 8 combinations of the Pacific and Atlantic patterns for the 5 AGCMs (see Table 1).

Figure 9: The regions of the United States used to form the averages in Figures 10 and 11.

Figure 10: Seasonality of the signal to noise ratios ( $R$  –see text) of the 3-month mean precipitation responses for each model over various regions of the United States to the Pacific warm (red curves) and cold (blue curves) SST anomaly pattern. The numbers along the abscissa refer to the center month of the 3-month means. Results are based on 50-year simulations except for the GFS model (dashed lines), which was run for 35 years. See text for the definition of the signal-to-noise ratio. The thin horizontal lines denote the 5% significance levels based on a t-test (for the GFS model the critical t-value is 0.49). Units: dimensionless.

Figure 11: Seasonality of the signal to noise ratios ( $R$  –see text) of the 3-month mean surface temperature responses for each model over various regions of the United States to the Pacific warm (red curves) and cold (blue curves) SST anomaly pattern. The numbers along the abscissa refer to the center month of the 3-month means. Results are based on 50-year simulations except for the GFS model (dashed lines), which was run for 35 years. See text for the definition of the signal-to-noise ratio. The thin horizontal lines denote the 5% significance levels based on a t-test (for the GFS model the critical t-value is 0.49). Units: dimensionless.

Figure 12; : Left panels: The annual mean surface temperature response to the positive phase of the trend pattern. Right panels: The annual mean surface temperature response to a globally uniform SST warming of 0.16 °C. The uniform warming run was not performed with CAM3.5. Units: °C.

Figure A1: Top panels: The second REOF and PC of the low pass filtered (time scales greater than 6 years) monthly SST data. Bottom panels: The first REOF and PC of the high pass filtered (time scales less than 6 years) monthly SST data. The results are based on the period 1901-2004. The values are scaled so that the product of the REOF and PC gives units of °C.

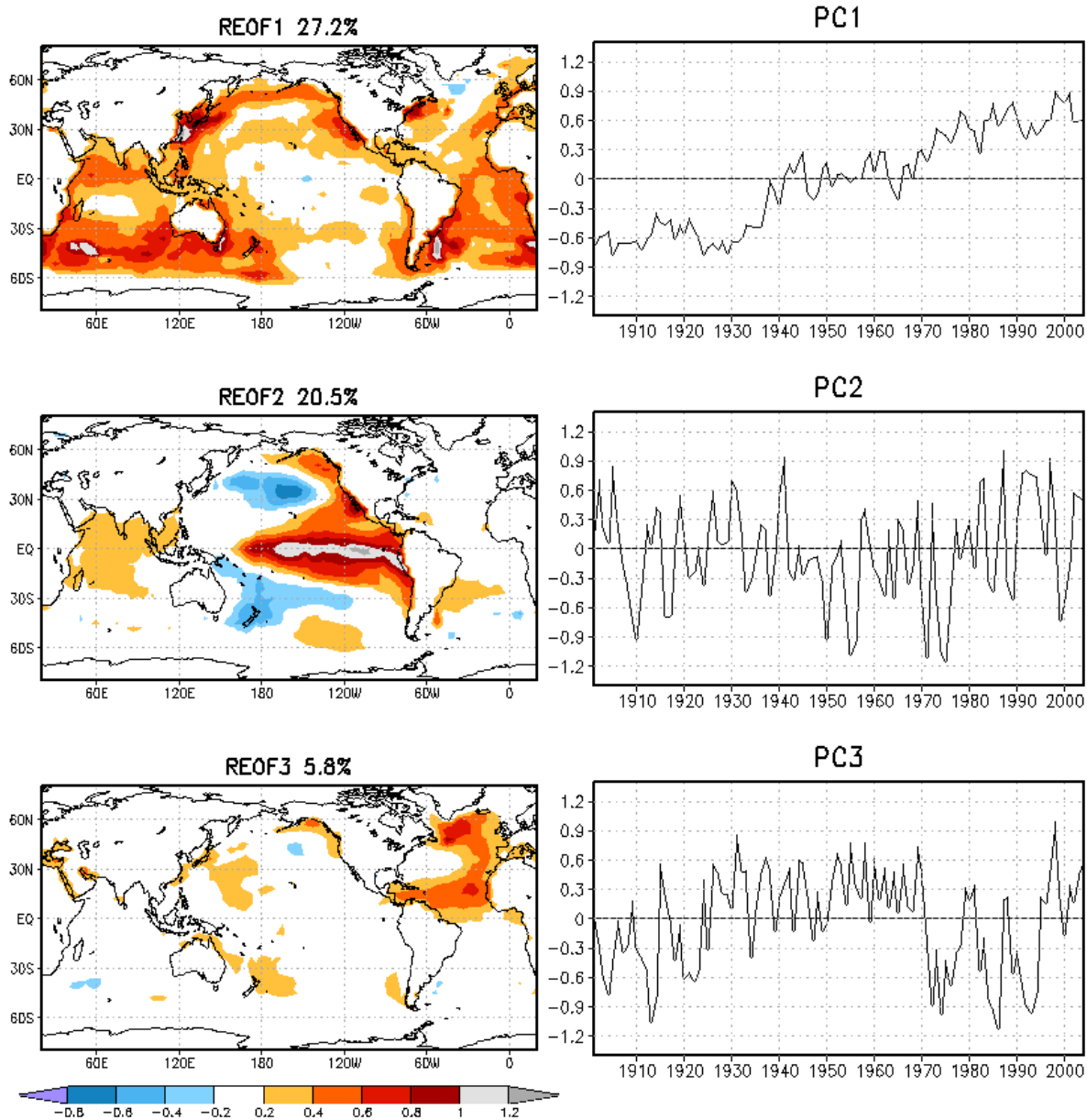


Figure 1: The three leading rotated EOFs (left panels) and associated PCs (right panels) of the annual mean SST based on the period 1901-2004. The values are scaled so that the product of the PCs and EOFs gives units of  $^{\circ}\text{C}$ . The Pacific and Atlantic patterns reflect the two standard deviation forcing amplitude applied to the models, while the trend pattern must be divided by a factor of two to obtain the forcing amplitude.

Clim Annual Precip (shaded) and Eddy Z200 (contour)

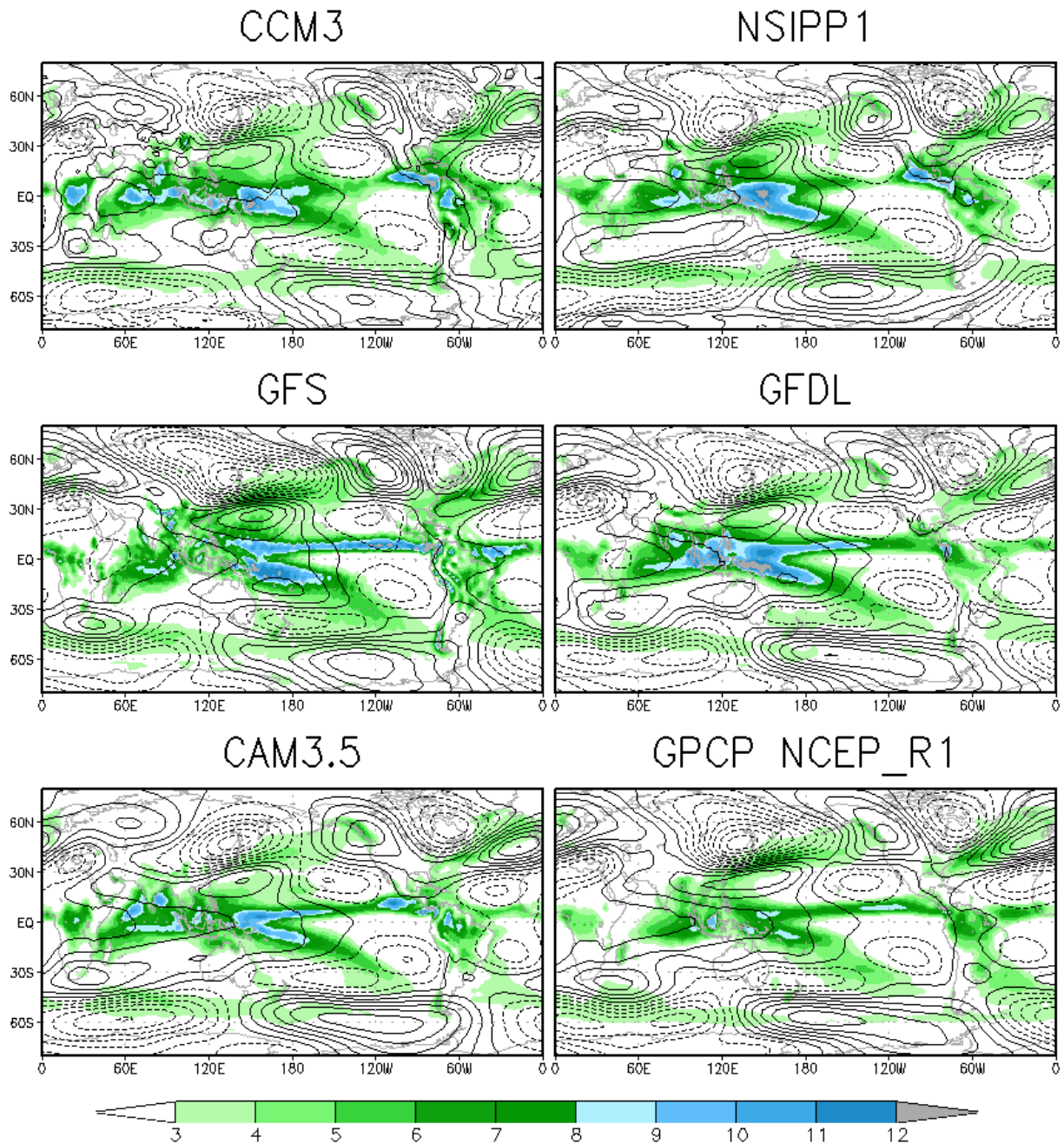


Figure 2: Annual mean precipitation and 200mb eddy height field averaged over the years 1980-1998. The model results are from AMIP-style runs from each model (runs forced by observed SSTs). For the observations (lower right panel), the precipitation is from GPCP (Adler et al. 2003) and the height fields are from the NCEP/NCAR reanalyses (Kalnay et al. 1996). The time period was chosen in order to have a common set of years for each model. Contour interval for the height field is 20m (negative values are dashed and the zero line is the first solid contour). Precipitation is in mm/day.

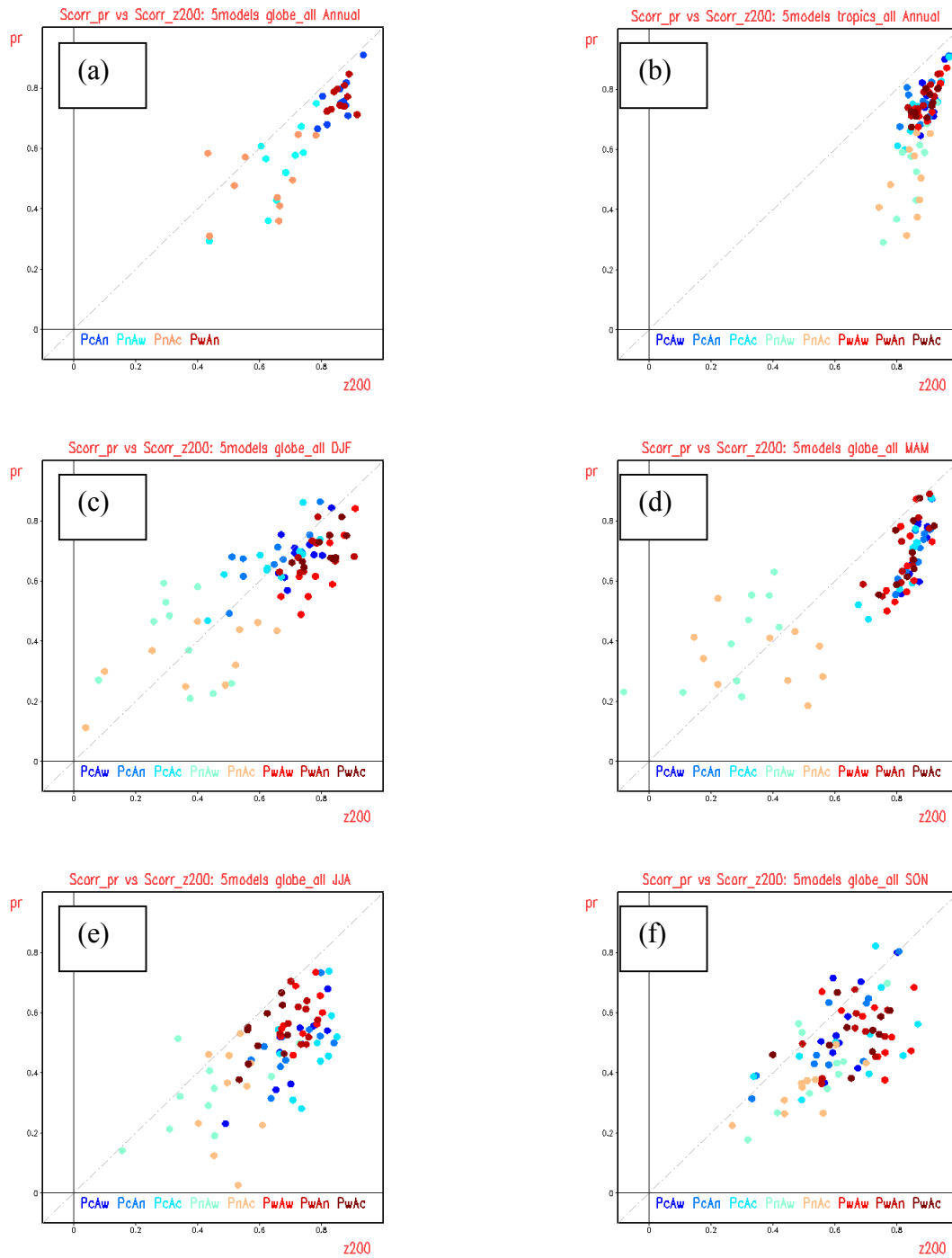


Figure 3: Spatial correlations of precipitation anomalies (ordinate) versus spatial correlations of 200mb height anomalies (abscissa) for the various combinations of models and for the various combinations of the Pacific and Atlantic forcing patterns. a) global correlations of annual means limited here to the 4 individual Pacific and Atlantic forcing patterns. b) tropical correlations ( $\pm 30^\circ$  latitude) of annual means, c) global correlations for DJF d) global correlations for MAM, e) global correlations for JJA, and f) global correlations for SON. See text for details. The colors refer to the forcing patterns indicated along the bottom of the plots.

Annual Mean precip\_z200 (WarmPac-Clim)

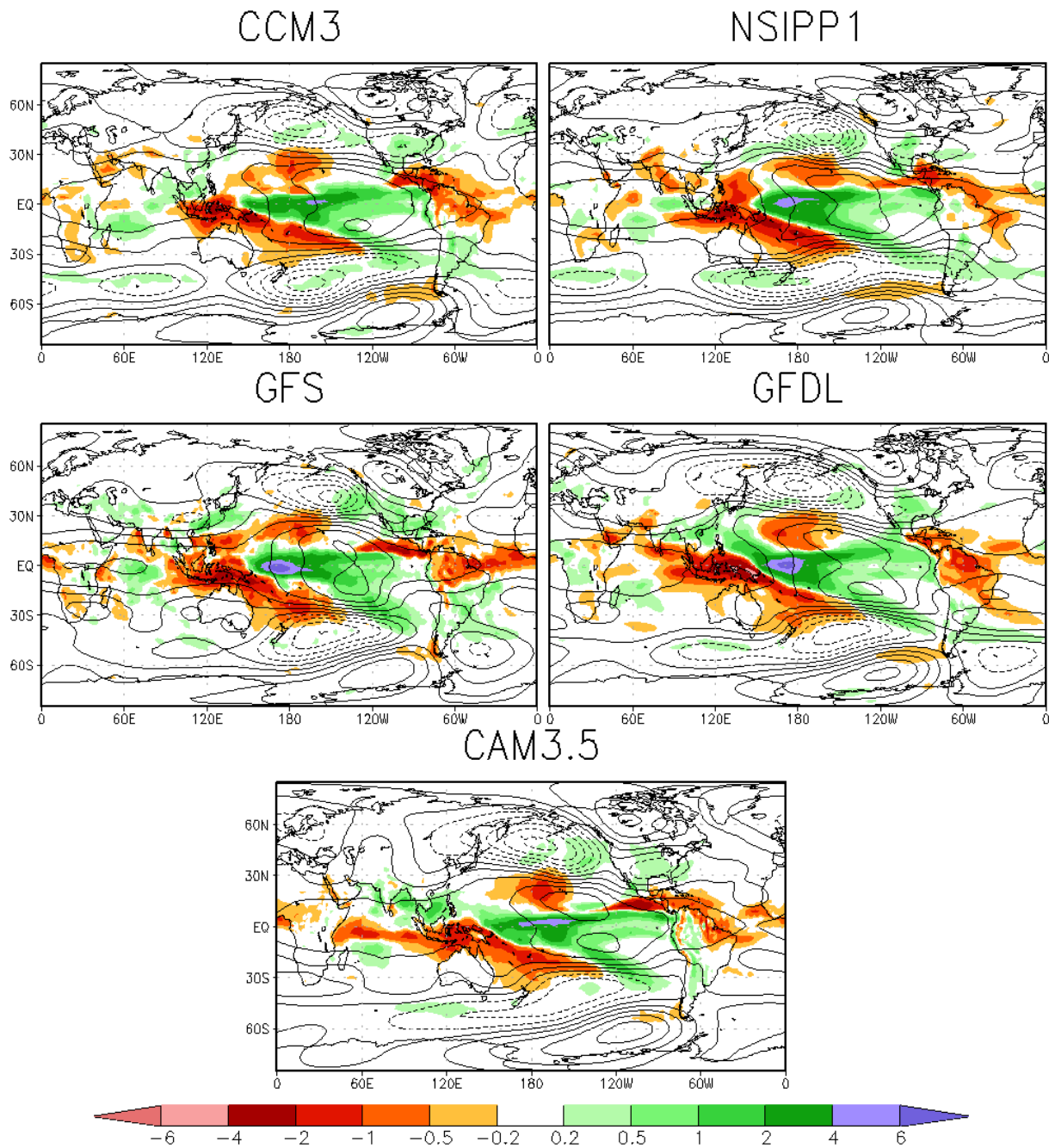
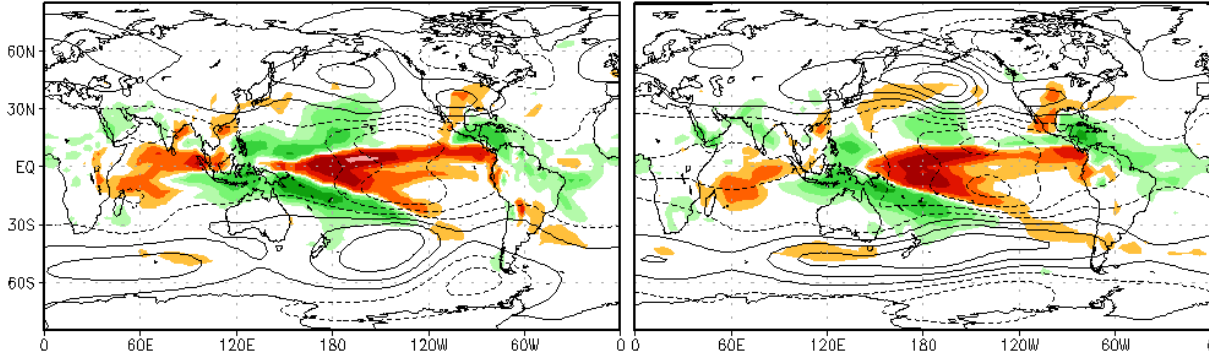


Figure 4: Annual mean 200mb height and precipitation responses to the of PwAn SST anomaly pattern. The anomalies for each model are computed with respect to its annual mean response to a simulation in which the model is forced with climatological SSTs. See text for details on the SST forcing. Contour interval for height is 10 meters (negative values are dashed and the zero line is the first solid contour). Unit for precipitation is mm/day.

Annual Mean precip\_z200 (ColdPac-Clim)

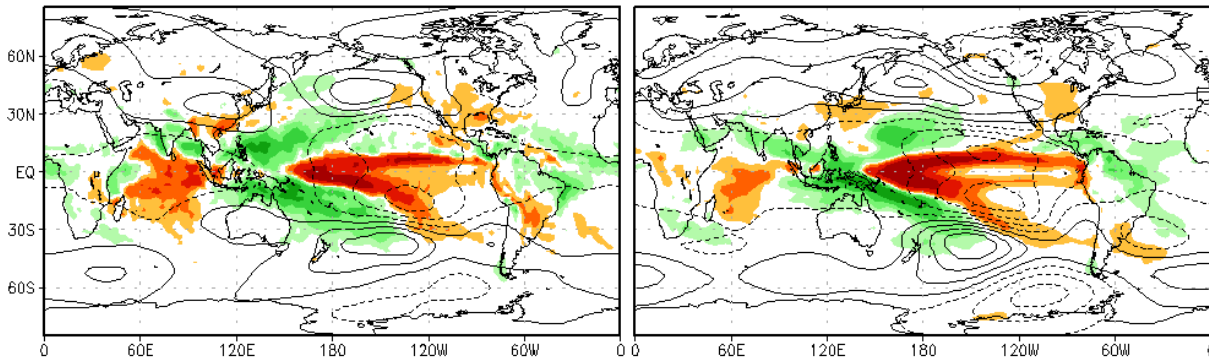
CCM3

NSIPP1



GFS

GFDL



CAM3.5

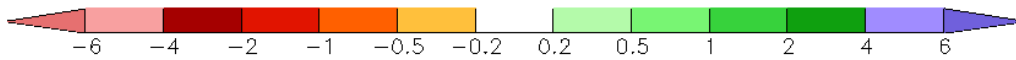
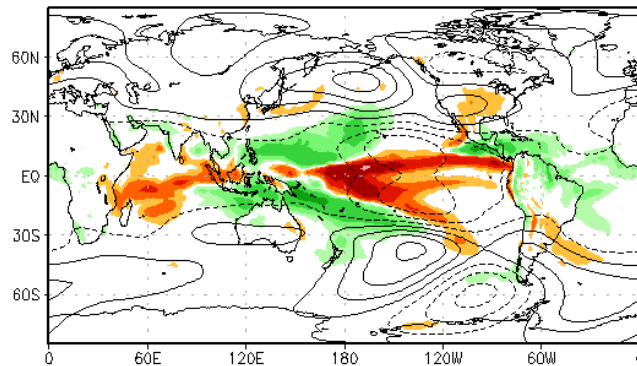


Figure 5: Annual mean 200mb height and precipitation responses to the of PcAn SST anomaly pattern. The anomalies for each model are computed with respect to its annual mean response to a simulation in which the model is forced with climatological SSTs. See text for details on the SST forcing. Contour interval for height is 10 meters (negative values are dashed and the zero line is the first solid contour). Unit for precipitation is mm/day.

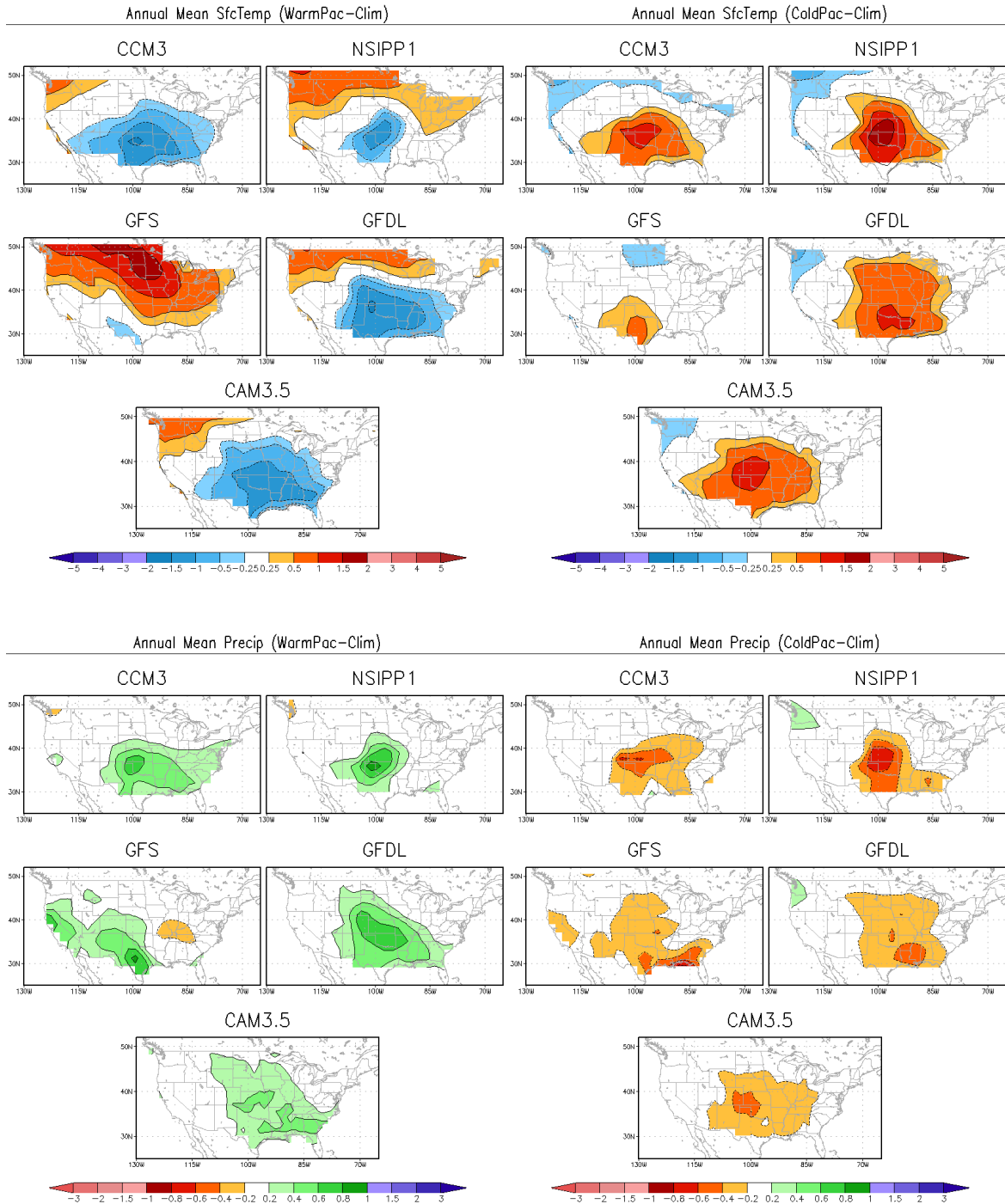


Figure 6: Annual mean surface temperature (top panels, units: °C/day) and precipitation (bottom panels, units: mm/day) responses to the PwAn (left panels) and PcAn (right panels) SST anomaly pattern. The anomalies for each model are computed with respect to its annual mean response to a simulation in which the model is forced with climatological SSTs. See text for details on the SST forcing.

Annual Mean Ptvstt\_GP (Pac-Clim)

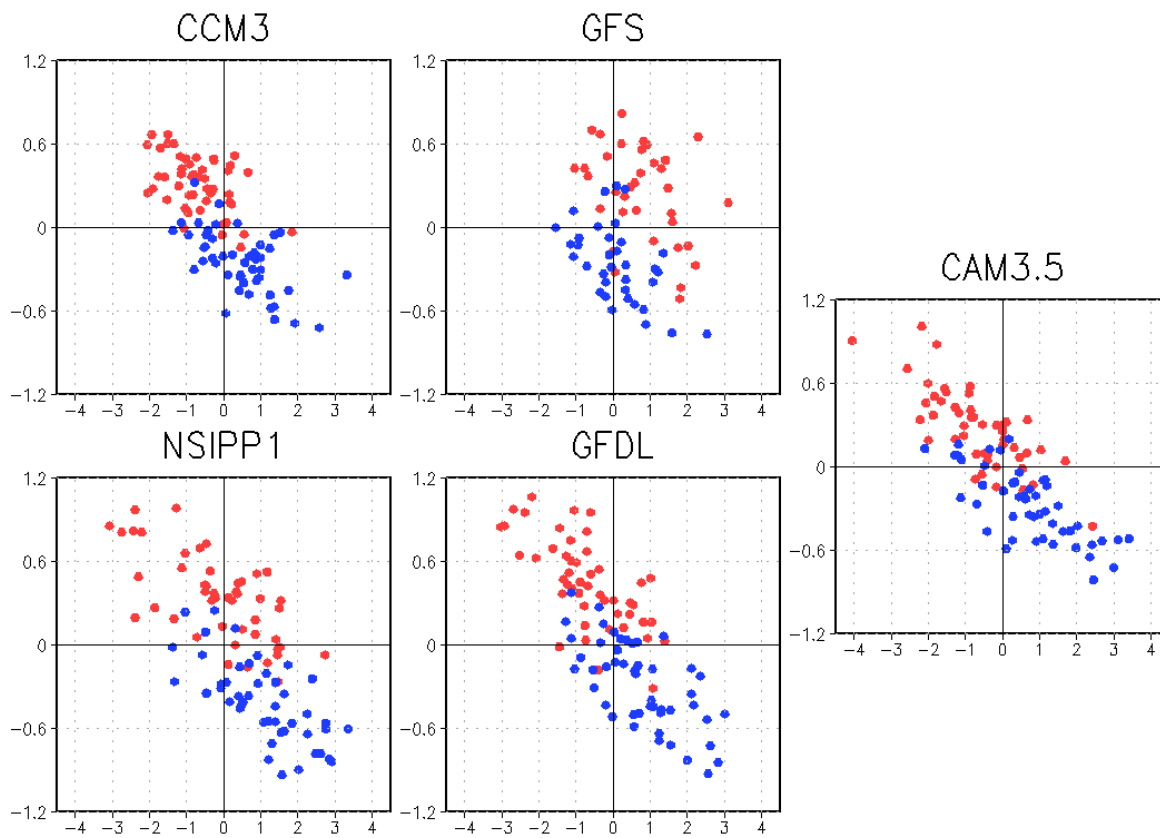


Figure 7: Scatter plots of the Great Plains annual mean precipitation (ordinate) versus surface temperature (abscissa) response to the PwAn (red dots) and PcAn (blue dots) SST anomaly patterns for the Great Plains area average. Each point represents one of 50 (35 for the GFS model) years of each run.

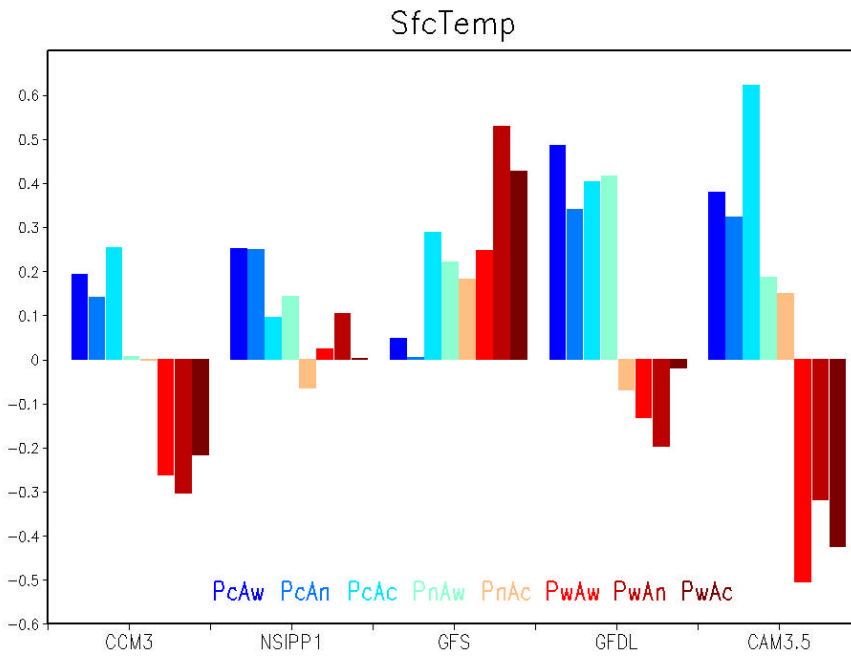
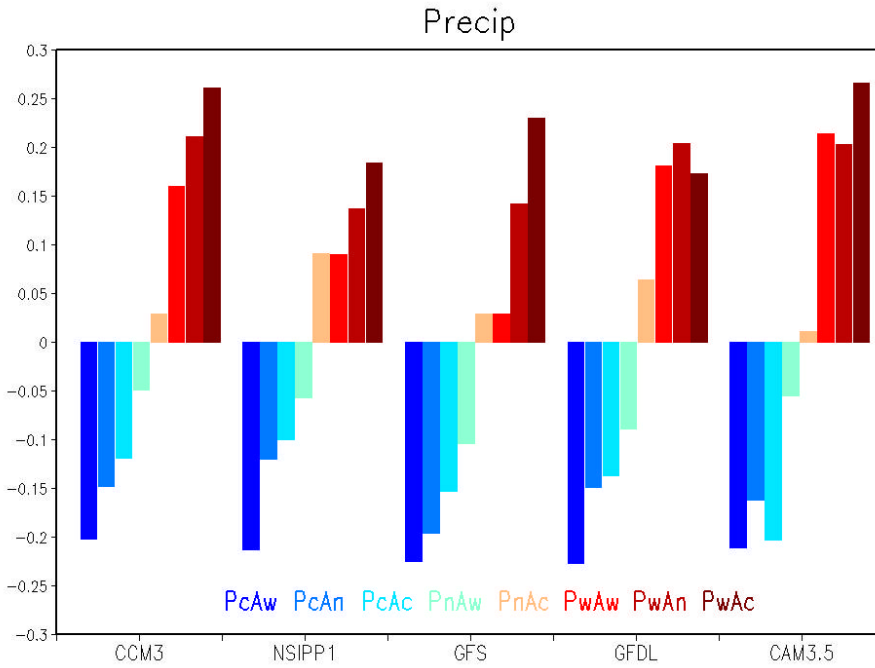


Figure 8: The annual and continental United States mean responses for a) precipitation and b) surface temperature for all 8 combinations of the Pacific and Atlantic patterns for the 5 AGCMs (see Table 1).

# U.S. Sub-regions

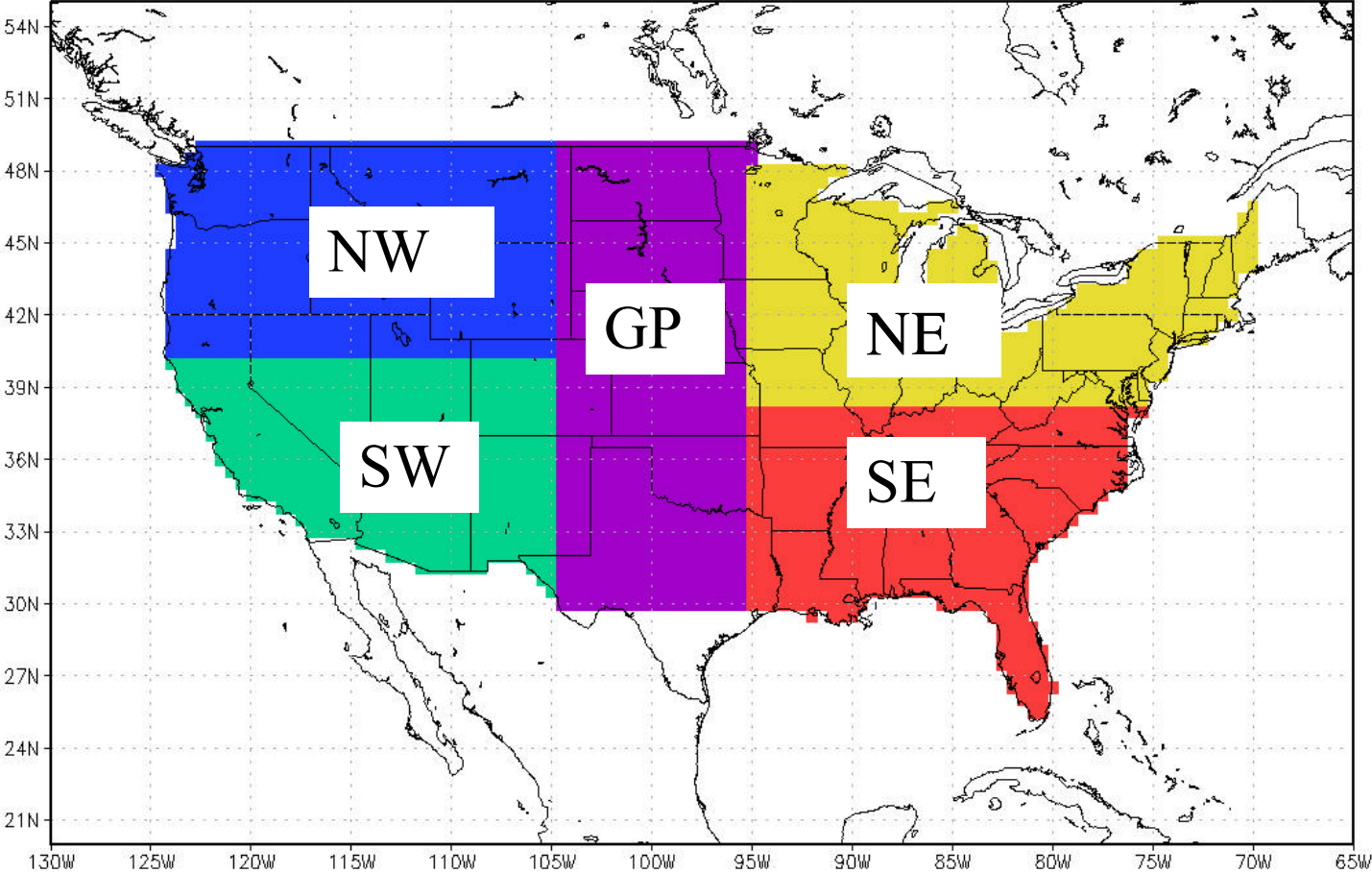


Figure 9: The regions of the United States used to form the averages in Figures 10 and 11.

Seasonality of Signal/Noise for Precip\_land Response over US subregions: Pac-Clim  
3-Mon RunMean

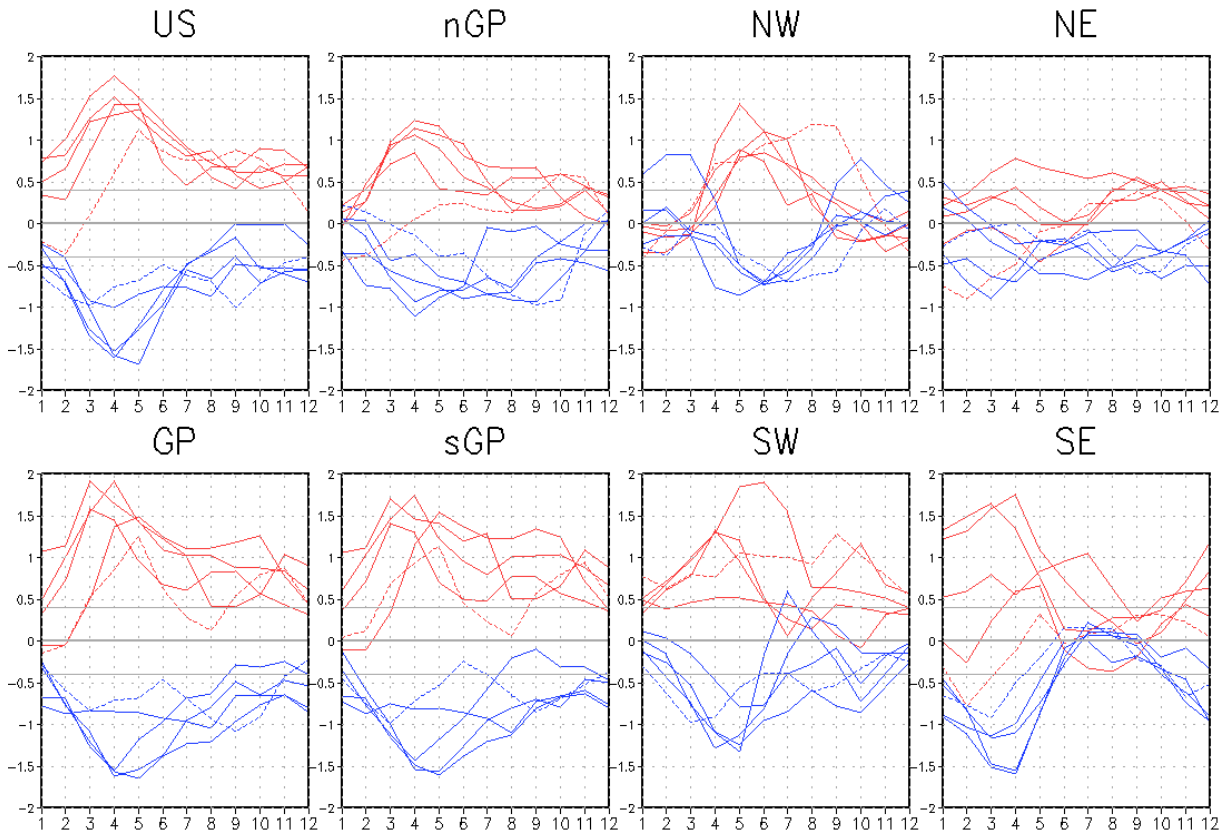


Figure 10: Seasonality of the signal to noise ratios ( $R$  –see text) of the 3-month mean precipitation responses for each model over various regions of the United States to the Pacific warm (red curves) and cold (blue curves) SST anomaly pattern. The numbers along the abscissa refer to the center month of the 3-month means. Results are based on 50-year simulations except for the GFS model (dashed lines), which was run for 35 years. See text for the definition of the signal-to-noise ratio. The thin horizontal lines denote the 5% significance levels based on a t-test (for the GFS model the critical t-value is 0.49). Units: dimensionless.

Seasonality of Signal/Noise for SfcTemp\_land Response over US subregions: Pac-Clim  
3-Mon RunMean

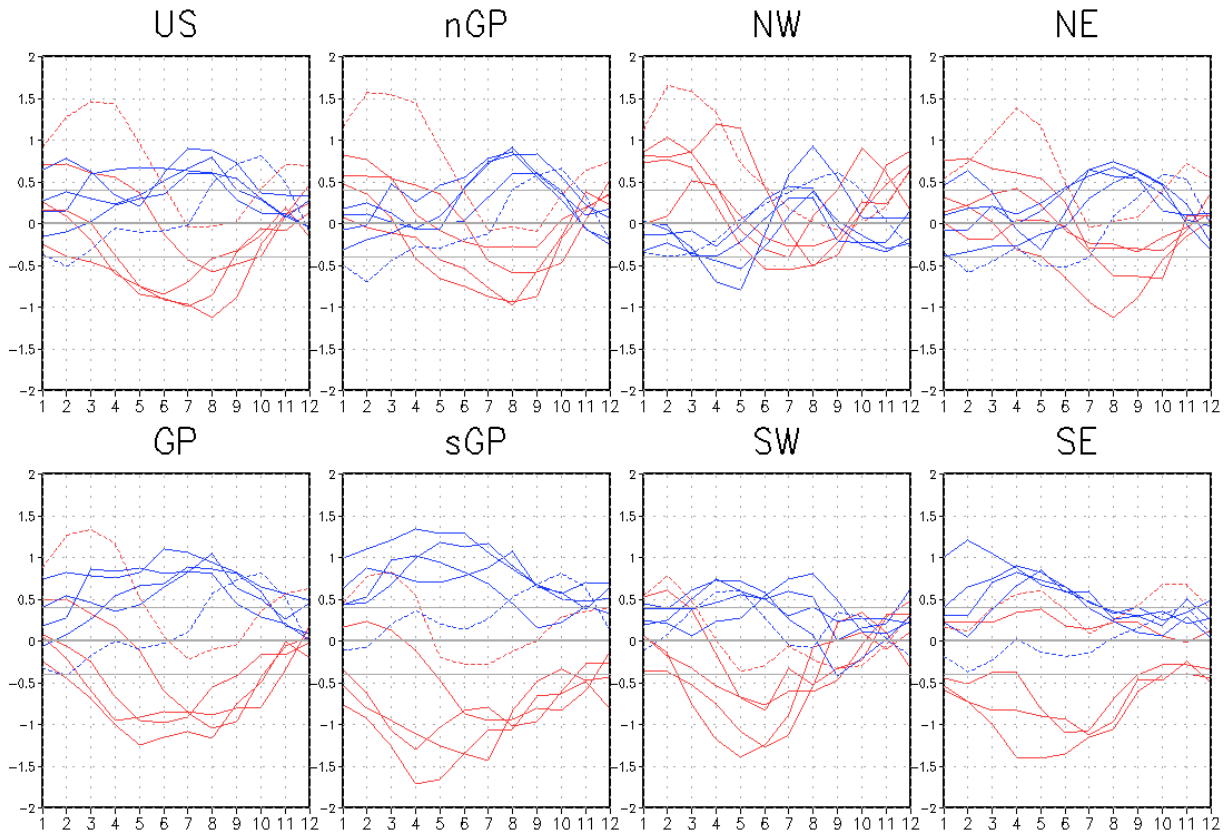


Figure 11: Seasonality of the signal to noise ratios ( $R$ —see text) of the 3-month mean surface temperature responses for each model over various regions of the United States to the Pacific warm (red curves) and cold (blue curves) SST anomaly pattern. The numbers along the abscissa refer to the center month of the 3-month means. Results are based on 50-year simulations except for the GFS model (dashed lines), which was run for 35 years. See text for the definition of the signal-to-noise ratio. The thin horizontal lines denote the 5% significance levels based on a t-test (for the GFS model the critical t-value is 0.49). Units: dimensionless.

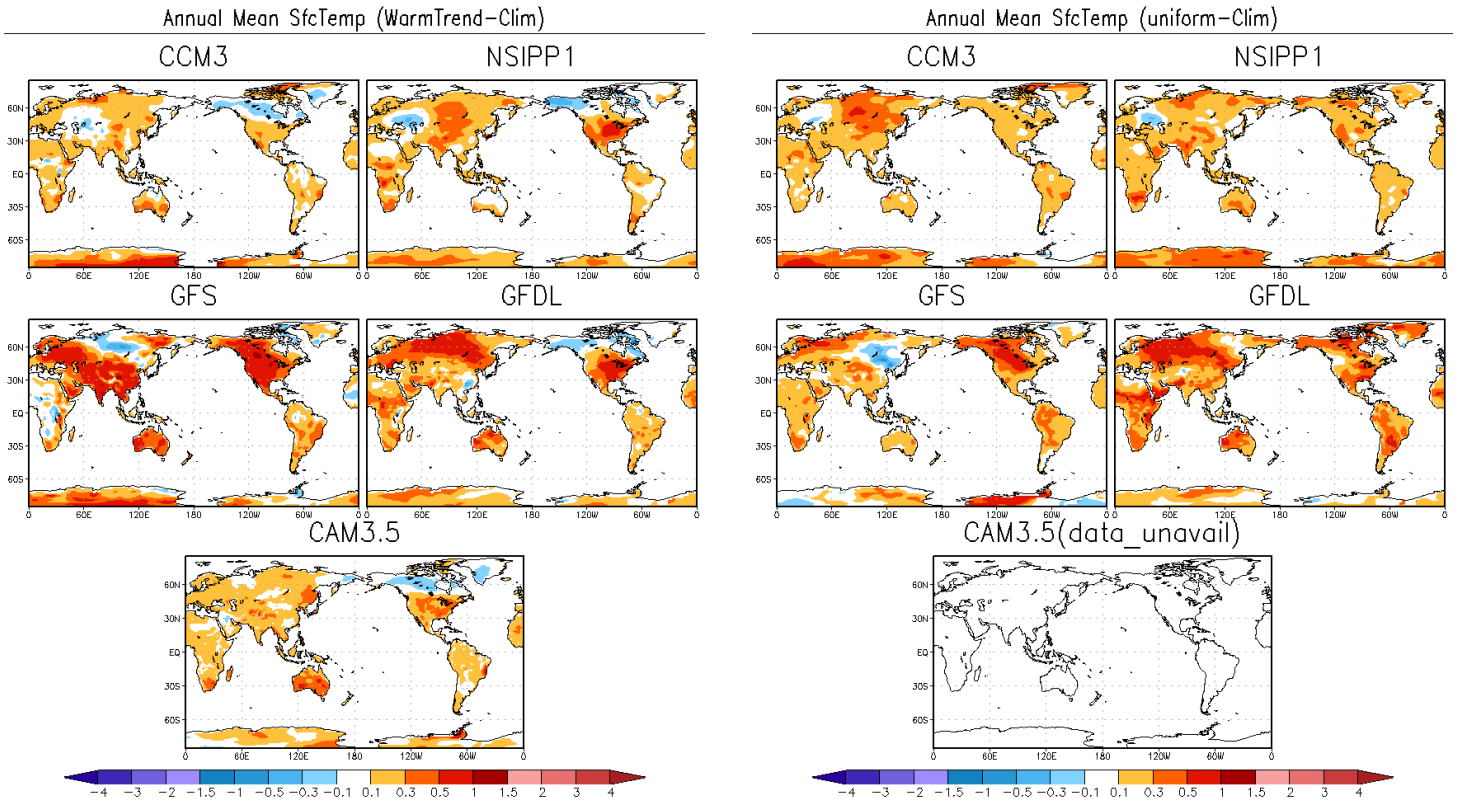


Figure 12: Left panels: The annual mean surface temperature response to the positive phase of the trend pattern. Right panels: The annual mean surface temperature response to a globally uniform SST warming of  $0.16\text{ }^{\circ}\text{C}$ . The uniform warming run was not performed with CAM3.5. Units:  $^{\circ}\text{C}$ .

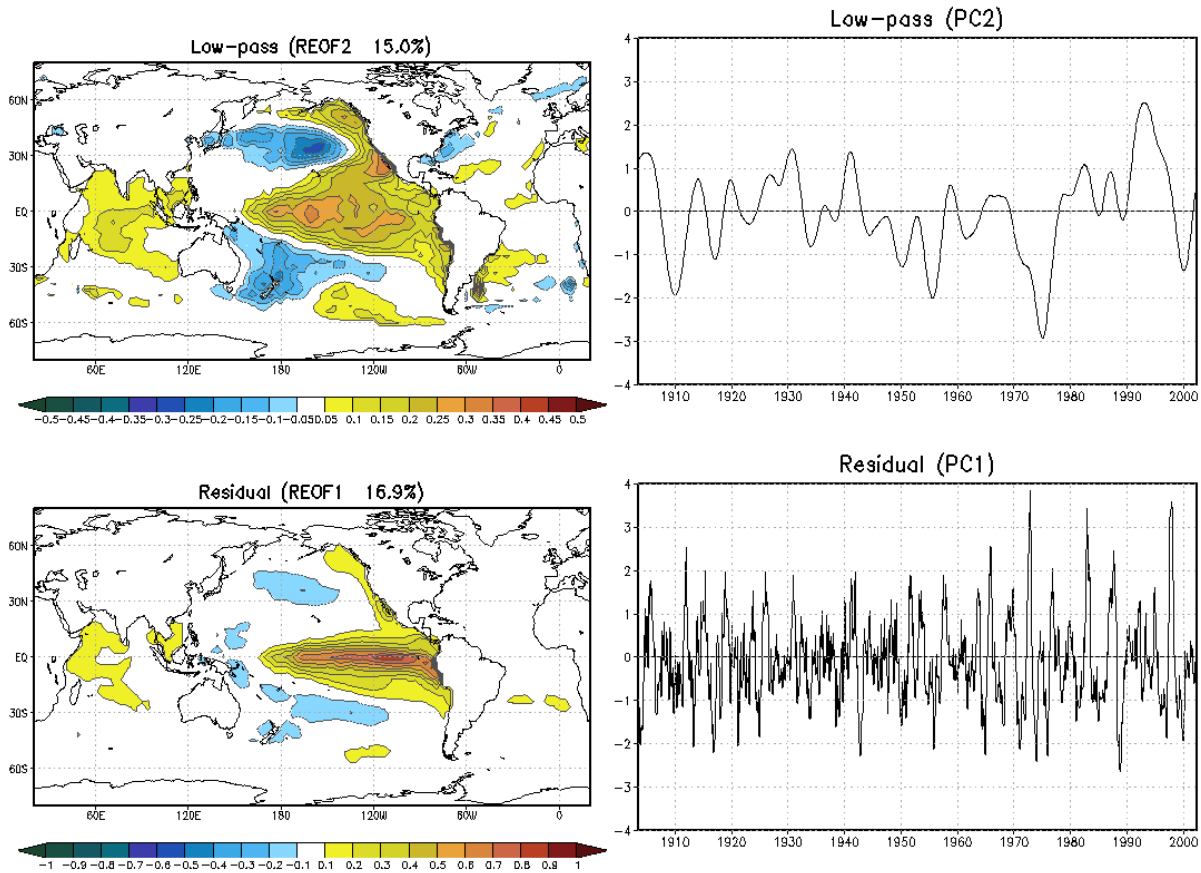


Figure A1: Top panels: The second REOF and PC of the low pass filtered (time scales greater than 6 years) monthly SST data. Bottom panels: The first REOF and PC of the high pass filtered (time scales less than 6 years) monthly SST data. The results are based on the period 1901-2004. The values are scaled so that the product of the REOF and PC gives units of °C.

Table 1: The different combinations of the *Pacific* and *Atlantic* SST anomaly patterns used to force the GCMs. Here *w* refers to the warm phase of the pattern (with a 2 standard deviation weight) and *c* refers to the cold phase (with a 2 standard deviation weight). Also, *n* denotes neutral indicating that the pattern has zero weight. In particular, the *PnAn* experiment denotes the control run forced with the annually-varying climatological SST.

	<b>Warm <i>Atlantic</i></b>	<b>Neutral <i>Atlantic</i></b>	<b>Cold <i>Atlantic</i></b>
<b>Warm <i>Pacific</i></b>	<i>PwAw</i>	<i>PwAn</i>	<i>PwAc</i>
<b>Neutral <i>Pacific</i></b>	<i>PnAw</i>	<i>PnAn</i>	<i>PnAc</i>
<b>Cold <i>Pacific</i></b>	<i>PcAw</i>	<i>PcAn</i>	<i>PcAc</i>

Table 2. Description of the models used in the drought working group simulations.

<b>Model</b>	<b>Resolution</b>	<b>Convection Scheme</b>	<b>Land Surface Model</b>
AM2p12 Delworth et al. 2006 GFDL Development Team (2004)	2° x 2.5°, L24	Relaxed Arakawa-Schubert (Moorthi and Suarez 1992)	Milly and Shmakin (2002)
GFS v2 Campana, K. and P. Caplan (2005)	T62 (~2°x2°), L64	Simplified Arakawa-Schubert (Grell 1993; Pan and Wu 1995)	Ek et al. (2003)
NSIPP-1 Bacmeister et al. (2000). Schubert et al. (2004)	3° x 3.75°, L34	Relaxed Arakawa-Schubert (Moorthi and Suarez 1992)	Mosaic (Koster and Suarez 1996)
CCM3.0 Kiehl et al. (1998) Seager et al. (2005)	T42 (~2.8° x 2.8°) with 18 hybrid sigma levels	Zhang and McFarlane (1995) Hack (1994)	Bonan (1996)
CAM3.5 <a href="http://www.cesm.ucar.edu/models/atm-cam/">http://www.cesm.ucar.edu/models/atm-cam/</a>	T85 with 27 hybrid sigma levels	Oleson et al. (2008)	Community Land Model Oleson et al. (2008) Stockli et al. (2007)
CCSM3.0 Collins et al. 2006	AGCM: T85 with 26 levels OGCM: 1°x1° telescoping to 1°x1/2° in deep tropics with 40 levels	Zhang and McFarlane (1995)	Community Land Model